ARMY RESEARCH LABORATORY

Measurements and Calculations of the Millimeter Wavelength RCS of a Top Hat and Bruderhedrals

by Joseph D. Silverstein and Robert Bender

ARL-TR-1281 March 1997

The findings in this report are not to be construed as an official Department of the Army position unless so designated by other authorized documents.

Citation of manufacturer's or trade names does not constitute an official endorsement or approval of the use thereof.

Destroy this report when it is no longer needed. Do not return it to the originator.

Army Research Laboratory
Adelphi, MD 20783-1197

ARL-TR-1281 **March 1997**

Measurements and Calculations of the Millimeter Wavelength RCS of a Top Hat and Bruderhedrals

Joseph D. Silverstein and Robert Bender
Sensors and Electron Devices Directorate

Abstract

Polarimetric radar cross sections (RCSs) were measured for a large top hat and three large Bruderhedrals at 35 and 93 GHz. The overall spread in the measured RCSs was 2 dB. It was found that the absolute RCS, as well as the dependence of the RCS on elevation angle, could be significantly altered by a slight misalignment of the target reflector. The calculations of these RCSs by theories and RCS simulation codes based on geometric and physical optics generally agreed with the measurements to within 3 dB. Radar calibrations using these reflectors, which are based on the predictions, are not reliable, however, if accuracy better than 3 dB is required. The measured values of the cross-polarization RCS were very small compared to the copolarization ones, consistent with theoretical predictions.

Contents

1. **Introduction** 1

2. **Top Hat and Bruderhedral RCS Predictions** 2
   - *2.1 Analytical Theories* 2
   - *2.2 Simulation Codes* 6

3. **Description of Measurements** 7
   - *3.1 Radars* 7
   - *3.2 Targets* 7
   - *3.3 Calibration* 9
   - *3.4 Target Positioning and Alignment Procedure* 10

4. **Measured Data** 13

5. **Comparisons of Measured Data With Predictions** 21
   - *5.1 RCS versus Elevation Angle* 21
   - *5.2 RCS versus Azimuthal Angle* 25

6. **Conclusions** 27

References 28

Acknowledgments 29

Appendix A.—Extension of Johansen's Theory 31

Distribution 33

Report Documentation Page 37

Figures

1. Top hat geometry and Bruderhedral geometry and their orientation relative to radar line of sight (RLOS) in terms of θ_{el} and θ_{az} 2
2. Measured data and theoretical predictions for RCS of Environmental Research Institute of Michigan (ERIM) top hat at 33 GHz and Ohio State University (OSU) top hat at 10 GHz 5
3. Top hat, bru01, bru02, and bru03, which also shows rotation bar covered with absorber 8
4. Schematic of reflector affixed to azimuth-over-elevation mount oriented for RCS versus θ_{el} measurements 11
5. RCS versus elevation angle measurements for bru01 at 93 GHz resulting from four different alignments 12
6. Measured top hat RCS versus elevation angle at 35 GHz and 93 GHz 14
7. Measured bru01a RCS versus elevation angle at 93 GHz 14
8. Measured bru01 RCS versus elevation angle at 35 GHz and 93 GHz 15
9. Measured bru03 RCS versus elevation angle at 35 GHz and 93 GHz 16
10. Bru02 RCS versus elevation at 35 GHz measured on different occasions 17
11. Bru02 RCS versus elevation at 93 GHz measured on different occasions 18
12. Measured bru01 RCS versus azimuthal angle at 35 GHz and 93 GHz 19
13. Measured bru02 RCS versus azimuthal angle at 93 GHz 19

14. Calculated RCS versus angle of RLOS to normal for 6- × 6-in. square plate at 35 GHz and 93 GHz 20
15. Measurements and predictions of top hat RCS versus elevation angle at 35 GHz and 93 GHz 21
16. Measurements and predictions of bru01a, HH RCS versus elevation angle at 93 GHz 22
17. Measurements and predictions of bru01, HH RCS versus elevation angle at 35 GHz and 93 GHz 22
18. Measurements and predictions of bru03, HH RCS versus elevation angle at 35 GHz and 93 GHz 23
19. Measurements and predictions of bru01, HH RCS versus azimuthal angle at 35 GHz and 93 GHz 26
20. Measurements and predictions of bru02, HH RCS versus azimuthal angle at 93 GHz 26

Tables

1. Parameters and RCS of reflectors 9
2. Comparison of measured maximum RCS to calculated maximum RCS 24
3. Overall comparisons of measured RCS to calculated RCS 24
4. Maximum VH RCS 25

1. Introduction

The top hat reflector, shown in figure 1(a), has been used as a convenient means of designating ground locations for airborne radars and calibrating various radar systems since the 1960s. However, the earliest citation of this reflector in the open literature is in a 1981 paper by E. L. Johansen [1]. That author describes the pros and cons of various configurations of the top hat, gives a formula for its radar cross section (RCS), and presents measurements of its RCS at 33 GHz that are consistent with his formula. Since that time, the top hat RCS has also been measured at 34 GHz [2] and 10 GHz [3]. The scattering from this reflector has been analyzed as well, based on physical optics [3] and on the geometric theory of diffraction and the method of moments [4]. Top hats continue to find use in the calibration of millimeter-wave (MMW) radars, particularly when the radars are polarimetric [2], since their polarimetric properties are simple and are theoretically identical to those of the plane dihedral [1]. The top hat has the advantage over the plane dihedral, however, in that its RCS changes slowly as a function of orientation angle in both the azimuthal and elevation planes.

In 1986, J. Bruder of the Georgia Institute of Technology introduced a reflector called a Bruderhedral [5], shown in figure 1(b). It is essentially a finite cylindrical segment of a top hat that retains the ease of orientation of the top hat, as shown by Bruder's measurements of the RCS patterns in both the elevation and azimuthal angle planes. The Bruderhedral is also predicted to have a higher RCS for its physical size than the top hat. The authors are aware of only one other measurement of RCS versus angle for the Bruderhedral, and only one analysis of the scattering from the reflector, which is based on the geometric theory of diffraction [4]. The Bruderhedral is now being used to calibrate MMW polarimetric radar systems [6,7].

A simple way of calibrating MMW polarimetric radars using Bruderhedrals is to simply align them for maximum return signal and assume that their absolute RCS is that calculated from the Johansen formula [1]. However, strictly speaking, that formula and even the Blejer theory (described in sect. 2.1), apply only to the top hat. Therefore, careful measurements on a variety of Bruderhedrals are needed to determine whether top hat RCS predictions also apply to the Bruderhedral. These needs motivated the measurements on three different Bruderhedrals, as discussed in this report. Measurements were also made on a top hat in order to have a baseline comparison of measurement to theory by which to rate the comparisons for the Bruderhedrals.

Section 2 describes the analyses and simulation codes used to calculate the reflectors' RCS. Section 3 describes the radars, targets, and measurement procedures. Section 4 then presents samples of the measured data, and section 5 compares the calculations with the measurements. Finally, section 6 presents some conclusions.

2. Top Hat and Bruderhedral RCS Predictions

2.1 Analytical Theories

Figures 1(a) and (b) define the basic geometric parameters of a top hat and a Bruderhedral, respectively. They also show the reflectors' assumed orientations in a set of *x*-, *y*-, and *z*-axes, and define the radar line of sight (RLOS), elevation angle θ_{el}, and azimuthal angle θ_{az} relative to those axes.

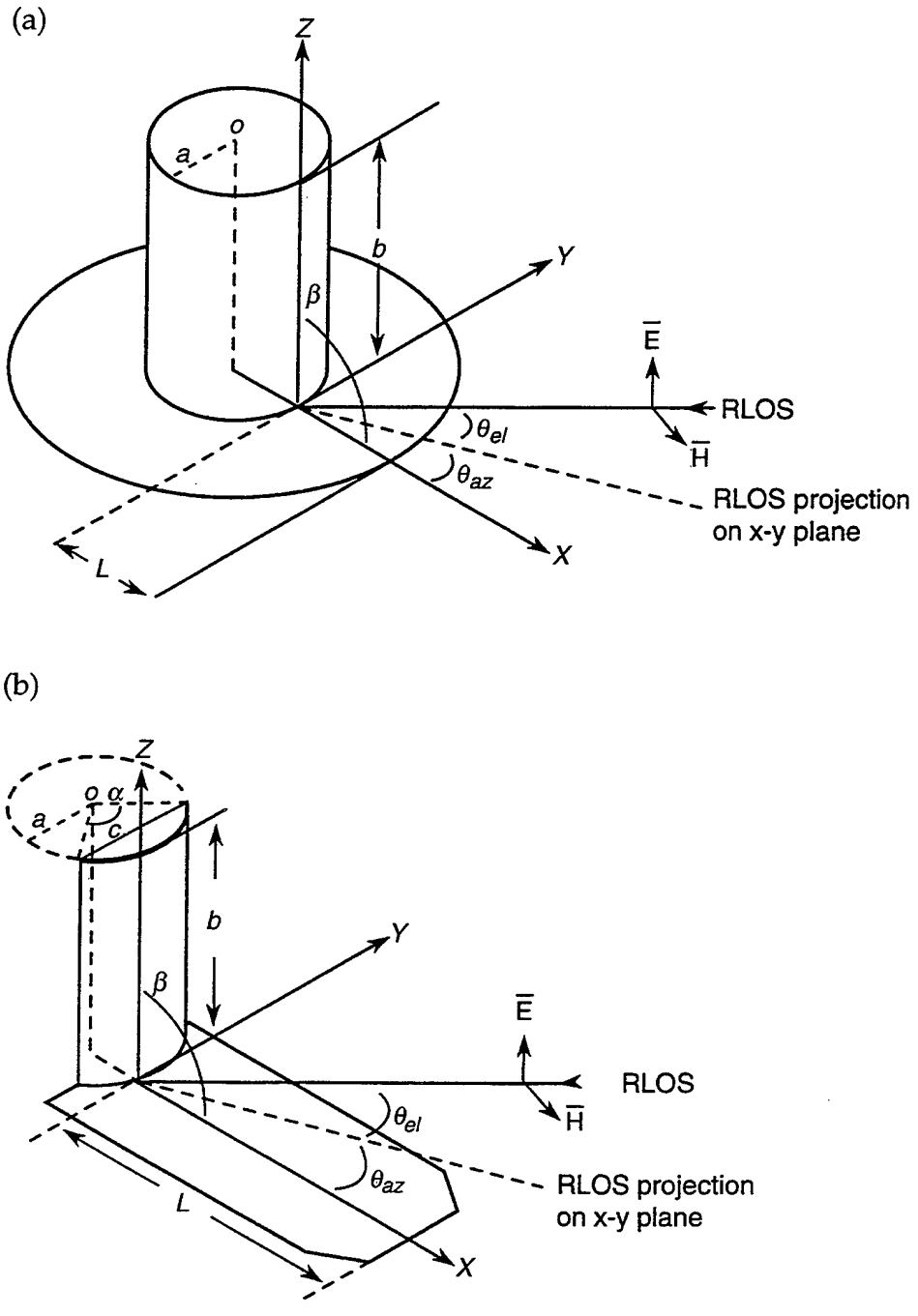

Figure 1. (a) Top hat geometry and (b) Bruderhedral geometry and their orientation relative to radar line of sight (RLOS) in terms of θ_{el} and θ_{az}.

Johansen based his simple formula for the RCS of a top hat [1] on the well-known "high-frequency" formula for the RCS of a finite right circular cylinder [8]:

$$\sigma = 2\,\pi ab^2/\lambda \ , \tag{1}$$

where a, b, and λ are the cylinder radius, cylinder length, and radar wavelength, respectively. Johansen's formula is*

$$\sigma = 8\pi ab^2 \cos(\theta_{el})/\lambda \ . \tag{2}$$

For the cylindrically symmetric top hat shown in figure 1(a), the RCS is independent of θ_{az}. As Johansen states, equation (2) is only valid for large elevation angles, such that

$$\tan(\theta_{el}) \geq b/L \ . \tag{3}$$

It is shown in appendix A that, based on the RCS of a finite right circular cylinder, the top hat RCS for small elevation angles, such that

$$\tan(\theta_{el}) \leq b/L \ , \tag{4}$$

is

$$\sigma = 8\pi aL^2 \tan^2(\theta_{el}) \cos(\theta_{el})/\lambda \ . \tag{5}$$

At the elevation angle for which

$$\tan(\theta_{el}) = b/L \ , \tag{6}$$

equations (2) and (5) both yield

$$\sigma = 8\pi ab^2 L/[\lambda (L^2 + b^2)^{1/2}] \ . \tag{7}$$

Equation (7) also gives the maximum RCS in both elevation angle regions.

Equation (2) is not valid near a 90-degree elevation angle, and equation (5) is not valid near a 0-degree elevation angle, since at those angles the single-bounce scattering from the plane base and cylindrical surfaces, respectively, predominates, and is not included in the simple Johansen theory. Since, as a calibration reflector, the top hat is usually used at elevation angles near the value of equation (6), where the return signal is maximized, the fact that these equations are invalid near 0 or 90 degrees should not present any practical limitation to using them for predicting the RCS of a top hat.

D. Blejer computed the complex polarization scattering matrix (PSM) for a top hat based on physical optics. A complex element of the PSM is denoted by S_{ij}, where i and j stand for H or V, denoting horizontal or vertical polarization, respectively, and the first and second subscripts denote transmit

**The formula for the top hat given by Bruder [5] differs from equation (2) due to an erroneous assumption in his derivation [9].*

and receive, respectively. In terms of S_{ij}, the RCS for the ij polarization channel is

$$\sigma_{ij} = \left| S_{ij} \right|^2 . \tag{8}$$

Blejer's PSM is diagonal. That is, S_{ij} is only nonzero for $i = j$, i.e., for the copolarization (copol) HH and VV channels. S_{ii} is given by

$$S_{ii} = S_{ii}^{ms} + S_{ii}^{cyl} + S_{ii}^{top} + S_{ii}^{gp} . \tag{9}$$

The first matrix element on the right-hand side of equation (9) is the contribution to S_{ii} from the multiple scattering between the cylinder and base, and the last three matrix elements are due, respectively, to the direct return from the side and top of the cylinder, and from the disc making up the ground plate, or base. For top hat dimensions that are small compared to λ, the three matrix elements impart a ripple to the RCS versus θ_{el} pattern, which arises from interference effects. However, for top hat dimensions that are large compared to λ, the magnitude of S_{ii}^{ms} is much larger than that of the other three matrix elements on the right-hand side of equation (9), except for θ_{el} near 0 and 90 degrees. If these three matrix elements are neglected in equation (9), the results for the HH and VV RCS given by equation (8) are the same, and are equal to the RCS in equation (2) or equation (5) from Johansen's theory, depending on whether θ_{el} satisfies equation (3) or equation (4), respectively.

Figure 2(a) compares the RCS measurements made by Johansen at 33 GHz on an Environmental Research Institute of Michigan (ERIM) top hat (a = 1.9 in., b = 12 in., L = 30 in.) to the Johansen and Blejer theories. Figure 2(b) compares the RCS measurements made by Ohio State University (OSU) at 10 GHz [3] on another top hat (a = 4 in., b = 8 in., L = 4 in.) with these theories. For θ_{el} between 0 and 10 degrees and between 80 and 90 degrees, the Blejer theory predicts rather large oscillations in the RCS, whereas the simple Johansen theory of equations (2) and (3), of course, does not. For the OSU top hat (fig. 2(b)), the oscillations predicted by the Blejer theory are much larger and extend farther in from θ_{el} = 0 degrees and θ_{el} = 90 degrees than for the ERIM top hat. As a result, in the former case the two theories coincide only to within 1 dB for θ_{el} between about 30 and 60 degrees. The larger and more extensive oscillations predicted by the Blejer theory for the OSU top hat than for the ERIM top hat are to be expected, since for the ERIM top hat a/λ = 5, b/λ = 34, and L/λ = 84, whereas for the OSU top hat a/λ = 3, b/λ = 7, and L/λ = 3. The ERIM top hat dimensions are much larger compared to λ than those of the OSU top hat. Therefore, the last three matrix elements on the right side of equation (7) are smaller compared to the first matrix element at a given θ_{el} near 0 or 90 degrees for the ERIM top hat than for the OSU top hat. One might be tempted to cite the absence of ripples in ERIM top hat measurements and the appearance of ripples in the OSU top hat measurements as conclusive support for the Blejer theory. However, the evidence based on the ERIM top hat measurements is not conclusive, since those data are wideband and result from a noncoherent averaging over 500 MHz [2]. Nevertheless, the agreement in

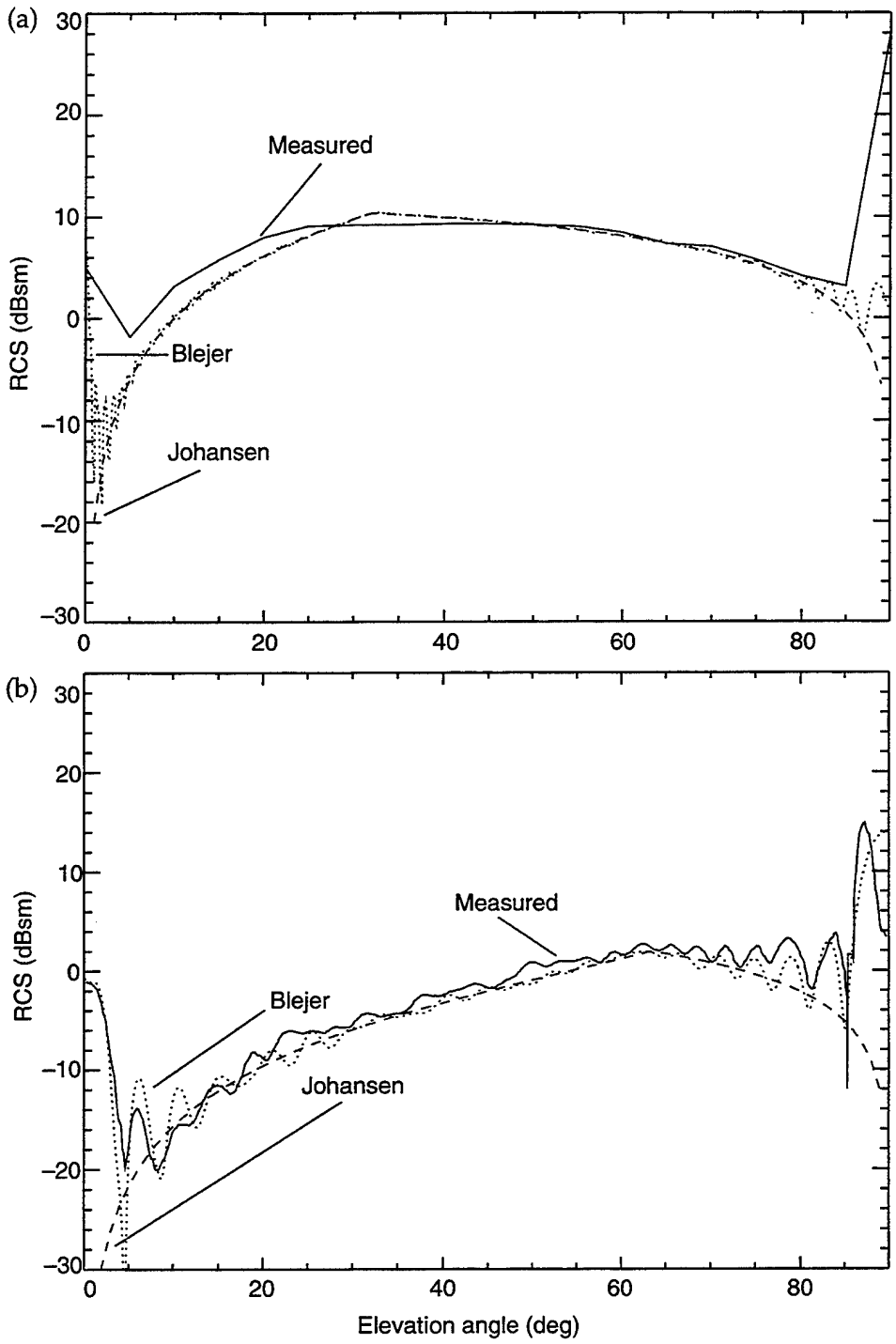

Figure 2. Measured data and theoretical predictions for RCS of (a) Environmental Research Institute of Michigan (ERIM) top hat at 33 GHz and (b) Ohio State University (OSU) top hat at 10 GHz.

figure 2(a) between the predictions of both theories and the measurements for the ERIM top hat is especially good, considering the fact that the base of this top hat, rather than being a disc of radius $a + L$ concentric with the cylinder, as in figure 1(a), was a long, rectangular plate, on which the cylinder was mounted with its axis a distance $a + L$ from the end of the plate facing the radar.

2.2 Simulation Codes

The RCS measurements reported in this paper were also compared with calculations of a number of radar simulation codes currently being used by radar systems designers. These codes were expected to yield results, for any given reflector, that are at least as accurate, if not more so, than those of the Johansen and Blejer theories. One reason for this expectation is that the codes employ geometric models that describe the actual shapes of the reflectors in much more detail than that afforded by the three geometric parameters, a, b, and L, used by the theories. Another reason is that the codes can include the effects of edge diffraction and shadowing, which the theories do not. It will be shown, however, that these expectations are not always realized.

The simulation codes tested were SRIM [10], xpatch [11], and GTS [12], all of which calculate the RCS of a target using the principles of geometric and physical optics. SRIM and xpatch ray trace a geometric model of the target by casting a bundle of parallel rays of the desired frequency on to it at the desired elevation and azimuthal angles and recording the histories of all multiple bounces up to some desired number. They then use this history to calculate the fields and currents on the target surfaces and, from these, the scattered fields, which determine the RCS.*

The models used for SRIM were of the constructive solid geometry (CSG) type and were built using the multiple-device graphics editor (MGED) modeling code contained in the Ballistics Research Laboratory computer-aided design (BRL-CAD) package [14]. The models used for the xpatch1 version of xpatch were faceted ones that were built either directly with the xpatch facet editor, or indirectly, with some other facet modeling code [15]. The models used for the xpatch2 version of xpatch were the same as those used in SRIM. Xpatch also has options allowing one to include specific computations of edge diffraction and ray divergence effects, using supplementary models, at the cost of additional computer time. GTS calculates the scattered field contributed from each of a number of primitives that are combined to form an approximation of the actual target shape. It uses a beam-trace technique to derive the multibounce scattering from targets and calculates edge diffraction effects, using a supplementary target model.

**The simulations performed by SRIM, however, may not be appropriate for the reflectors measured in this work. The reason is that these simulations neglect any rays impinging first on the cylindrical surface that diverge due to the curvature of that surface, but still hit the flat base surface in such a way that they could contribute to the RCS [13].*

3. Description of Measurements

3.1 Radars

The RCS of the reflectors was measured with two noncoherent, fully polarimetric radars mounted side by side at a height of about 8 m. They operated at frequencies of 35 and 93 GHz. The radars transmitted 10-W peak power, 60-ns pulses at a repetition rate of 50 kHz, and could measure returns from targets at ranges between 30 and 60 m. A boxcar integrator averaged the received signal over 1000 samples. Motorized, precision, 0- to 50-dB attenuators were connected to the output of the impact avalanche transit time (IMPATT) generating the rf power. The attenuators were used to calibrate the receiver channels and to limit the transmitted power when the return from a target overloaded those channels. A mechanical waveguide switch after the attenuator allowed the transmit polarization to be set to either vertical or horizontal by means of an orthomode transducer and a Faraday rotator. The latter elements also channeled the vertically and horizontally polarized components of the return signal to the vertical and horizontal receive channels, respectively.

The operations of the radars involved in obtaining a complete RCS versus angle pattern were controlled by a program running on a Hewlett-Packard (HP) 9000 series computer. These operations included setting the attenuator, operating the waveguide switch to transmit the proper polarization, and setting the gate delay. This program computed a raw datum every 0.05 degree of target rotation to minimize the effects of statistical fluctuations. The program also performed all the computations necessary to obtain absolute calibrations of the raw data (see sect. 3.3). The amplitudes of the signals in both receivers in the selected range gate were displayed on a digital voltmeter. In addition, the returned pulses could be observed on an A-scan display. These displays were especially useful for properly aligning the targets with respect to the RLOS (see sect. 3.4).

The radars were mounted on an elevation-over-azimuth positioner to enable them to be aimed at some selected target. A television camera was also mounted on the positioner and was selectively boresighted with one or the other of the radars to aid in properly aiming that radar at the desired target.

3.2 Targets

The RCSs of a top hat and three Bruderhedrals were measured. These reflectors are shown in figure 3. The Bruderhedrals (fig. 3(b-d)) will be referred to in this paper as bru01a or bru01, bru02, and bru03, respectively. Bru01a is an early version of bru01 in which the angle, β, between the cylindrical segment and base was 89.6 degrees. For bru01, this angle was corrected to 90 degrees. Figure 1 defines the geometrc parameters of the top hat and Bruderhedrals. They are the cylinder radius, a, cylinder height, b, base length, L, measured outward from the crease, and, the angle β.

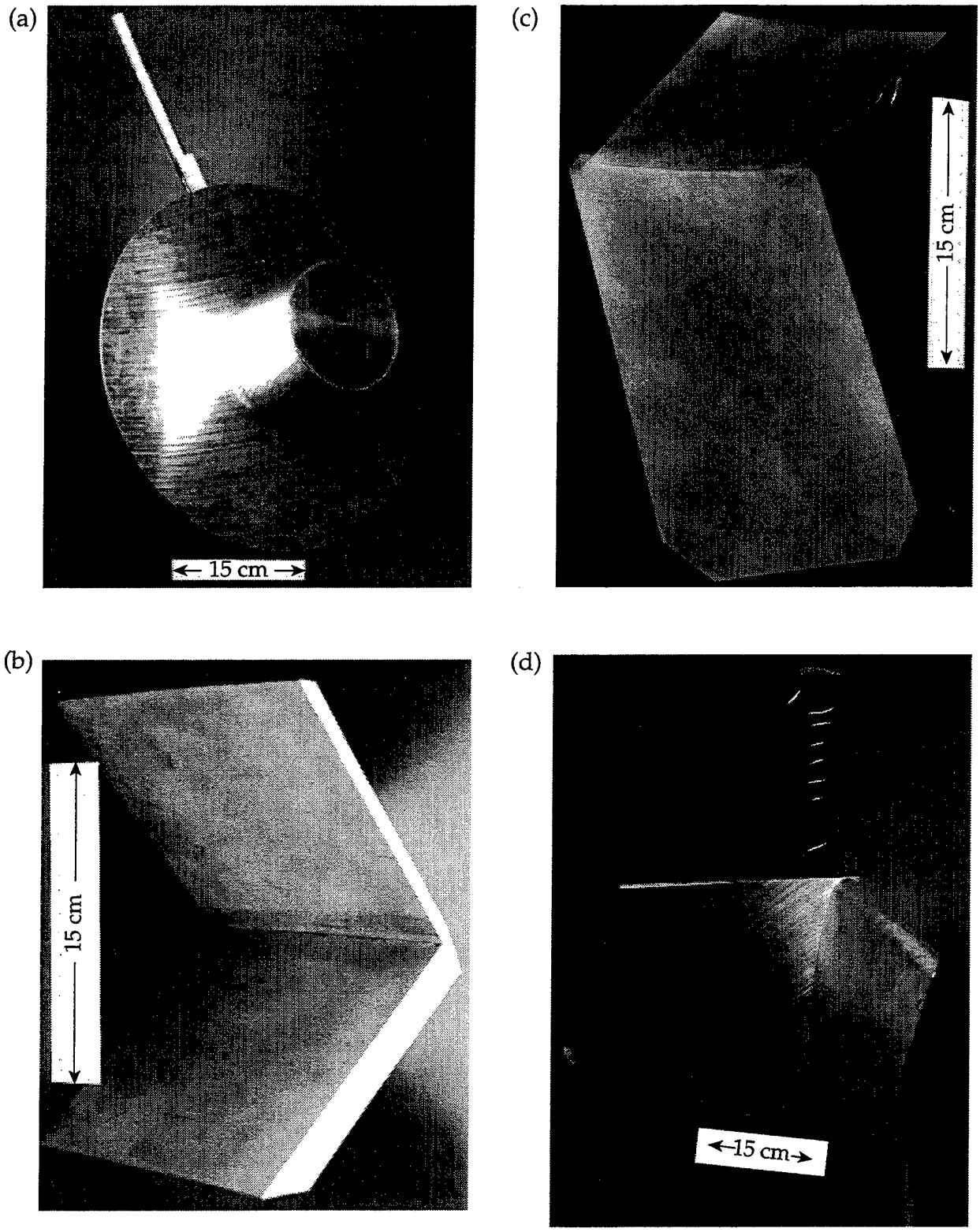

Figure 3. (a) Top hat, (b) bru01, (c) bru02, and (d) bru03, which also shows rotation bar covered with absorber.

Figure 1(b) for the Bruderhedral also shows the chord length, c, defined by the cylindrical segment and the angle, α, subtended by this segment. Table 1 gives the values of these parameters. It also gives the predictions of θ_{el} for maximum RCS (eq (6)) and the maximum RCS (eq (7)) of the reflectors at 35 and 93 GHz, according to Johansen's theory, assuming that that theory can be applied to Bruderhedrals as well. Bru01a and bru03 had been previously fabricated in-house for use as calibration reflectors [7]; bru02 was obtained commercially [16], and the top hat was fabricated in-house especially for the measurements reported in this work. The upper boundary of the cylinder segments of all the Bruderhedrals are knife edges formed by rear surfaces, that slope abruptly downward. These surfaces are sloped rather than horizontal to prevent any scattering from them from interfering with scattering due to just the cylindrical and flat base surfaces. In addition, the side boundaries of the cylinder sections of bru01 and bru02 are also knife edges for similar reasons. However, in bru03 the side boundaries of the cylinder section are terminated with segments of 0.75-in.-radius cylinders, which were located tangent to the 26-in.-radius cylinder segment to ensure a continuous, smooth surface.

The target was mounted on top of an 8-m-high telephone pole at a range of 47 m from the radars. It was rotated by a steel or aluminum mounting rod to which it was clamped. The crease of the top hat and Bruderhedrals could be oriented by eye at any angle relative to the mounting rod.

3.3 Calibration

A triangular trihedral was mounted on top of another 25-ft-high pole, also located 155 ft from the radars. This pole was far enough from the target pole to be well outside the radar footprint when the radar was aimed at the target. The triangular trihedral was used to determine an absolute RCS calibration for the copol VV and HH channels by measurements of the trihedral's RCS. That RCS was measured by comparing the trihedral's return signal with that from a right circular cylinder target mounted on the

Table 1. Parameters and RCS of reflectors.

Quantity	Top hat	bru01a	bru01	bru02	bru03
a/λ at 35 GHz	9	233	233	89	77
b/λ at 35 GHz	18	18	18	18	38
L/λ at 35 GHz	18	18	18	28	40
c/λ at 35 GHz	NA	18	18	18	42
Maximum RCS at 35 GHz (dBsm)*	6	20	20	17	22
a/λ at 93 GHz	24	620	620	237	204
b/λ at 93 GHz	48	47	47	48	102
L/λ at 93 GHz	48	47	47	76	107
c/λ at 93 GHz	NA	47	47	48	110
Maximum RCS at 93 GHz (dBsm)*	10	24	24	21	26
α (°)	NA	4	4	11	16
β (°)	90.0	89.6	90.0	89.9	90.0
Angle of maximum RCS (°)	45	46	46	32	44

**Johansen theory prediction*

target pole and perfectly aligned with its cylindrical surface normal to the RLOS. For this cylinder, a = 3.0 in. and b = 5.9 in. Since these dimensions are large compared to λ at 35 and 93 GHz, its RCS could be calculated to a high degree of accuracy from equation (1). The measured values of the trihedral's RCS were 10.5 and 18.6 dBsm at 35 and 93 GHz, respectively.

A second large triangular trihedral was mounted on a tripod far removed from both the target and absolute calibration trihedral poles. It was used to obtain calibration curves for the vertical and horizontal receive channels of the radars. A dynamic range of 50 dB was obtained for the calibration curves, with the average of the return signals from the trihedral measured before and after each target measurement session, and with the absolute trihedral RCS, which was measured as described above. The result was signal versus absolute RCS curves for the copol channels. Such curves will henceforth be referred to as absolute calibration curves. The accuracy of these calibrations is estimated to be between 0.5 and 1.0 dB.

The calibration of the cross-polarization (xpol) VH and HV channels relative to that of the copol channels was determined by comparing the signals returned from a triangular trihedral with those from a plane dihedral. These reflectors were mounted successively on the target azimuth-over-elevation table, and aligned with their axes of symmetry parallel to the RLOS. The RCS of these targets at millimeter wavelengths can also be accurately computed from well-known "high-frequency" formulas [5]. As mentioned above, the trihedral returns signals to the copol channels only. Therefore, by varying the attenuation of these signals, absolute calibration curves for the copol channels were, once more, obtained. The plane dihedral was then mounted, and its crease was rotated in a plane perpendicular to the RLOS until the signals in the xpol channels were maximized relative to those in the copol channels. That maximization is known to occur when the crease is at an angle of 45 degrees relative to the polarization vector [5]. The differences between the dihedral RCS, in dBsm, computed from the formula and that corresponding to the dihedral xpol signals determined from the absolute calibration curves then gave the offsets, in decibels, of the VH channel RCS from the HH channel RCS, and of the HV channel RCS from the VV channel RCS.

3.4 Target Positioning and Alignment Procedure

Figure 4 is a schematic showing how the reflectors were positioned by an azimuth-over-elevation mount located at the top of the telephone pole. The reflector was clamped to the mounting rod, which was, in turn, permanently mounted perpendicular to the azimuthal rotation table of the mount. For RCS versus θ_{el} measurements, the reflector was clamped to the mounting rod with the plane of its base parallel to the axis of the mounting rod, as shown in figure 4. For RCS versus θ_{az} measurements, which were performed only for the Bruderhedrals, the reflector was clamped so that the plane of its base was at about a 45-degree angle to the axis of the mounting rod. As stated in section 3.2, both those mounting positions were accomplished only with the aid of the eye.

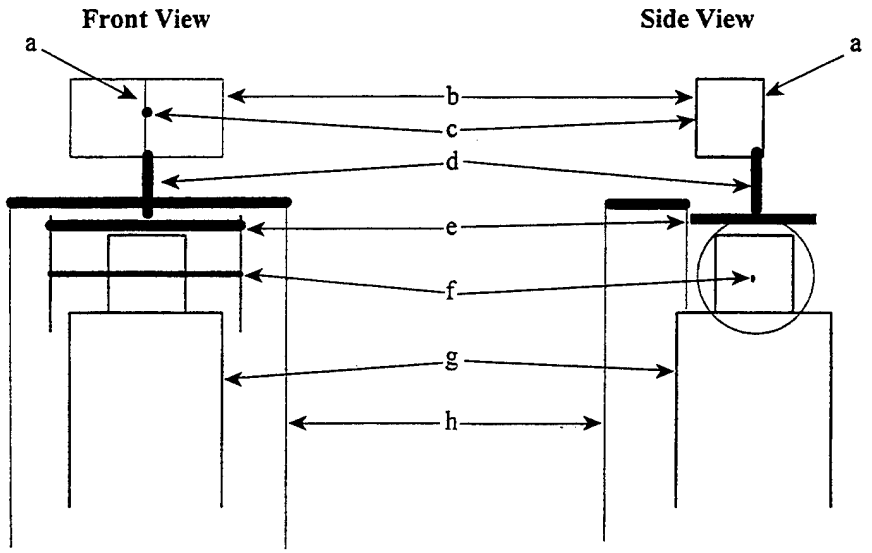

Figure 4. Schematic of reflector affixed to azimuth-over-elevation mount oriented for RCS versus θ_{el} measurements. Callouts: a–reflector crease; b–reflector; c–RLOS; d–table azimuthal axis and mounting rod lined with absorber; e–rotation table lined with absorber; f–table elevation axis; g–telephone pole; and h–sheet metal scattering shield capped with absorber.

For measurements of RCS versus θ_{el} at a fixed θ_{az} the target was aligned either with its flat surface normal to the RLOS ($\theta_{el} = 90°$), or with its crease normal to the RLOS ($\theta_{el} = 45°$). We accomplished the first of these alignments by looking for an A-scan display "flash," and the second one by looking for a maximum pulse height on a digital voltmeter, while making fine adjustments to the orientations of the target table. In actuality, more than one flash or pulse height maximum could be observed during these adjustments, each of which could sometimes result in a significantly different RCS versus elevation angle pattern. This is illustrated in figure 5, which shows RCS versus θ_{el} patterns for bru01 obtained by aligning the target on a flash and on various pulse height maxima. We obtained patterns in figures 5(a) and 5(b) that are very similar to each other, by aligning bru01 on a flash and on a pulse height maximum, respectively, which occurred at almost exactly the same elevation axis position of the table. The patterns in figures 5(c) and 5(d), however, are quite different. We obtained them by aligning bru01 on pulse height maxima other than that in figure 5(b). Since the elevation axis positions of the target table for the data in figures 5(a) and 5(b) were almost identical and gave rise to almost identical patterns, it was assumed that one or the other of them should be used for aligning the target in order to obtain the "true" pattern. It is quite likely that some of the anomalous results obtained for the shapes and amplitudes of the RCS patterns during the course of these measurements occurred because of incorrect alignment. Similar misalignment effects have been observed in RCS versus θ_{el} measurements of a top hat [2].

If the value of the flash signals saturated the receive channels, attenuation was inserted into the rf path to reduce the signal to just below the saturation level. This attenuation was present during all subsequent measurements of the target and absolute calibration trihedral.

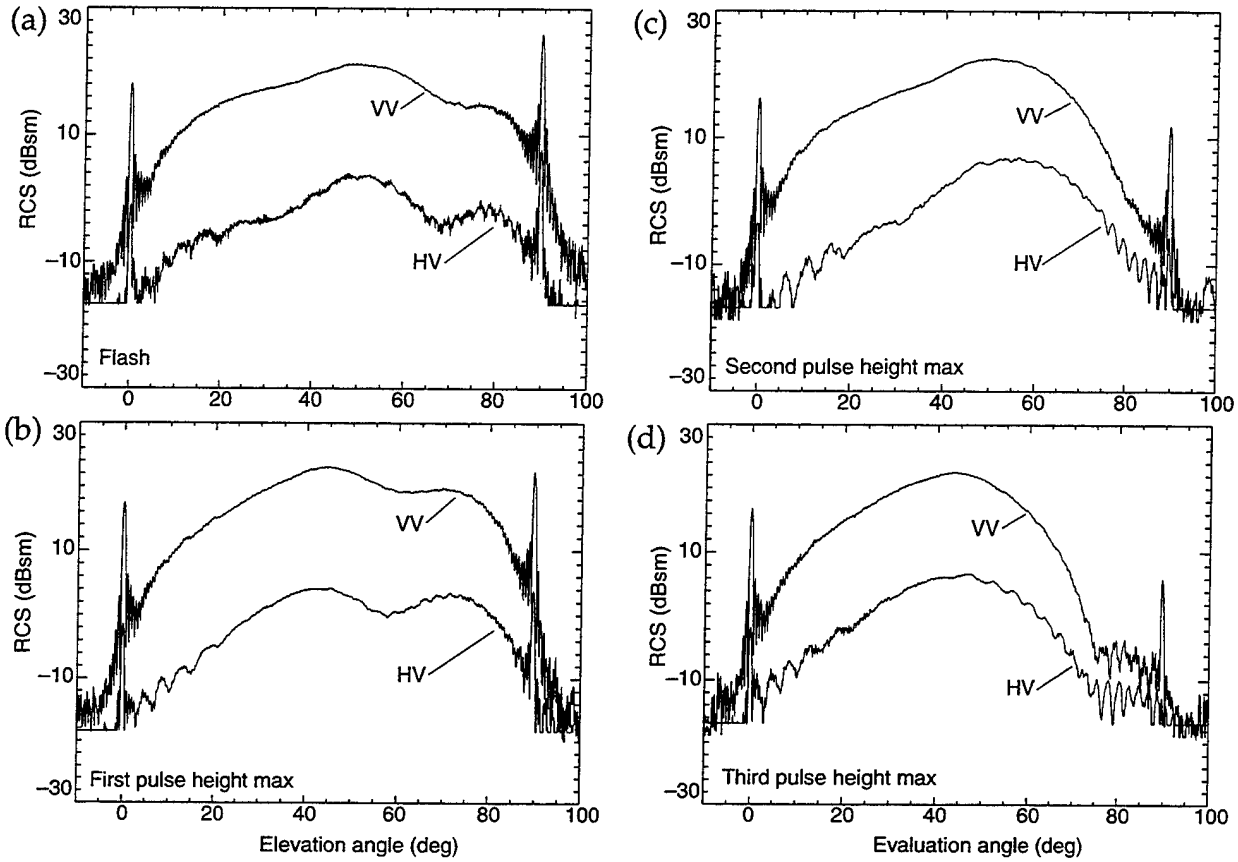

Figure 5. RCS versus elevation angle measurements for bru01 at 93 GHz resulting from four different alignments.

Since the RCS of the top hat and Bruderhedrals varies very slowly with θ_{az} when θ_{el} is far from 0 or 90 degrees, there were no alignment procedures available corresponding to those described above for measurements of RCS versus θ_{az} at a fixed θ_{el}. The alignment consisted of merely adjusting the elevation axis of the mount so that θ_{el} had a value of approximately 45 degrees.

Figure 4 shows that the mounting rod, rotation table, and the top of the scattering shield were covered with absorber to prevent signals from contaminating the data (see fig. 3(d)).

4. Measured Data

While the 35-GHz radar could transmit either horizontally or vertically polarized waves, its receiver could only receive horizontal polarization. The result was that only HH and VH data could be collected at 35 GHz. The measurements of RCS versus elevation angle for HH and VH were performed a number of times for each target on different days during the course of about a six-month period. In most cases, the shapes of those patterns repeated fairly well, and the amplitude had a total spread of about 2 dB or less. Figures 6, 7, 8, and 9 show representative RCS versus θ_{el} data obtained for the top hat, bru01a, bru01, and bru03, respectively, at $\theta_{az} = 0$ degrees. The RCS versus θ_{el} data obtained for bru02, however, were not repeatable. Figures 10 and 11 each show measurements on bru02 made in the same manner on two different occasions. It is possible that these inconsistencies may, at least in part, be due to misalignment of the reflector, which was discussed in section 3.4. The HH and VV patterns for each of these targets were usually identical, and their HV and VH patterns were quite similar in both shape and amplitude at 93 GHz.

Figure 6 for the top hat clearly shows the flashes from the cylinder and base at 0 and 90 degrees, respectively. A 180-degree interval was sampled; the top hat data began at a slightly negative θ_{el} and ended at an elevation angle slightly less than 180 degrees. Therefore, only the flash off the cylinder at $\theta_{el} = 0$ degrees is seen. The oscillatory nature of the top hat data, especially at 35 GHz (fig. 6(a)), is not understood and will be discussed in section 5. It was often found that the amplitude of these oscillations was larger when windy conditions prevailed.

The copol bru01 pattern at 35 GHz in figure 8(a) and the copol patterns for bru03 at 35 and 93 GHz in figure 9 all have rather smooth, bell shapes. The copol patterns for bru01a in figure 7 and that for bru01 in figure 8(b) are identical in shape and amplitude. This result differs from the results of calculations of the effects on the RCS of dihedrals of deviations of its angle β from 90 degrees [5]. Those calculations yield a 3-dB reduction in RCS at 93 GHz when β is 89.6 degrees rather than 90 degrees. Unlike the other copol patterns mentioned above, those in figures 7 and 8(b) have a broad dip between 55 and 75 degrees superimposed on the bell shape. Such a dip is also evident in the RCS versus θ_{el} data measured by Bruder [5]. If the top hat theories discussed in section 1 also apply to the Bruderhedral, then, as expected on the basis of equation (6) (since $b = L$ is satisfied exactly, or nearly so, for all of the reflectors except bru02), their RCS maxima should occur at or near $\theta_{el} = 45$ degrees (see table 1). This is seen to be the case for the data in figures 5 through 9. Based on all these data, when these reflectors are used to calibrate the copol channels of a radar, we would have to orient them in the elevation plane to within about 5 degrees of the angle of maximum RCS if we desired a calibration uncertainty of not more than 1 dB.

Figure 6. Measured top hat RCS versus elevation angle at (a) 35 GHz and (b) 93 GHz.

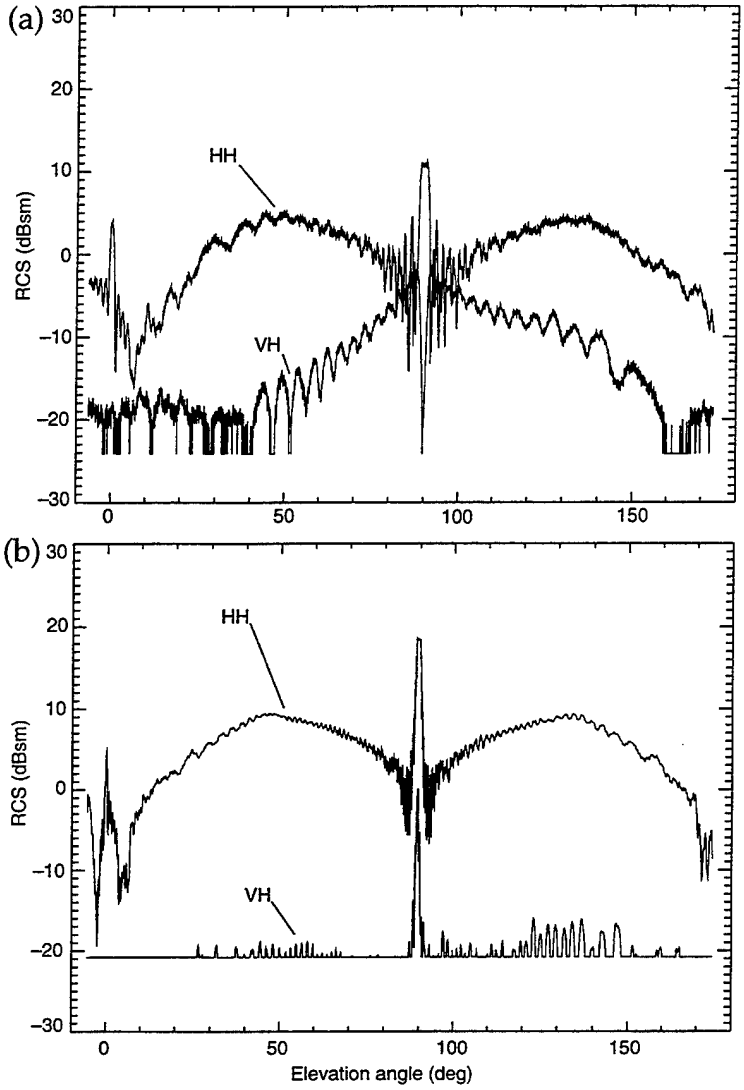

Figure 7. Measured bru01a RCS versus elevation angle at 93 GHz.

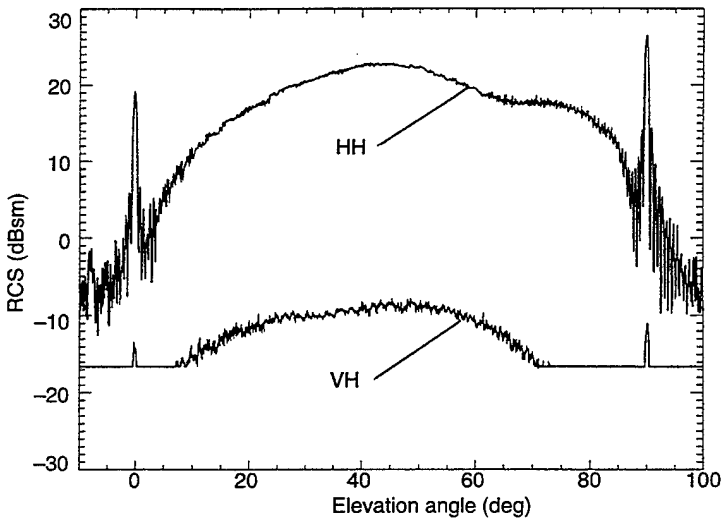

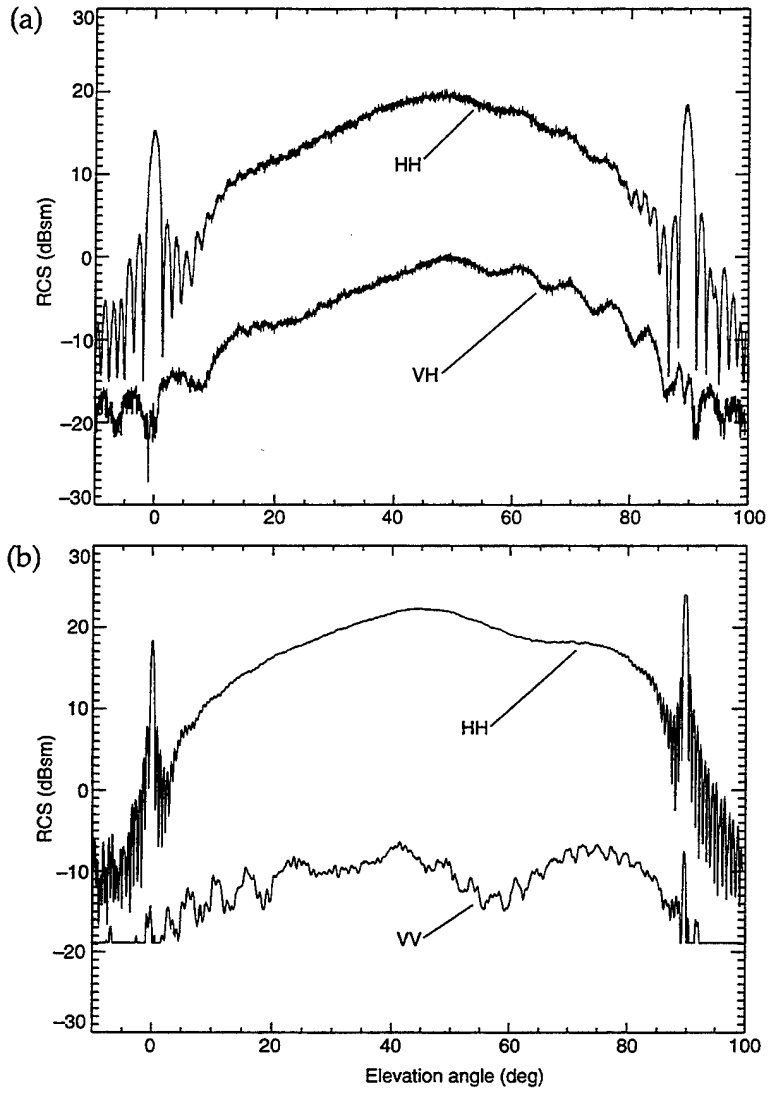

Figure 8. Measured bru01 RCS versus elevation angle at (a) 35 GHz and (b) 93 GHz.

For most of the data in figures 6 through 11, the xpol RCS is 20 dB or more down from the copol RCS at the same angle. The finite RCS measured in the xpol channels may be due to two sources. The first is the finite orthogonal polarization component transmitted by the radars, which is expected to be more than 20 dB down from that of the main component. The second trace is the slight misalignment of the mounting table axes relative to the polarization vectors of the radar beams. The xpol RCS of the top hat and Bruderhedrals is expected to be small, since the scattering mechanisms taking place in these reflectors are very similar to those of the plane dihedral. Complete geometric and physical optics analyses of the scattering from that reflector [17] yield almost purely diagonal PSMs when the crease in the dihedral is oriented parallel or perpendicular to the polarization vector, as was the case in these measurements. As stated in section 2, the physical optics treatment of the top hat by Blejer [3] resulted in a purely diagonal PSM. A physical optics treatment of the Bruderhedral might, therefore, yield off-diagonal PSM elements that are, if not zero, then very small.

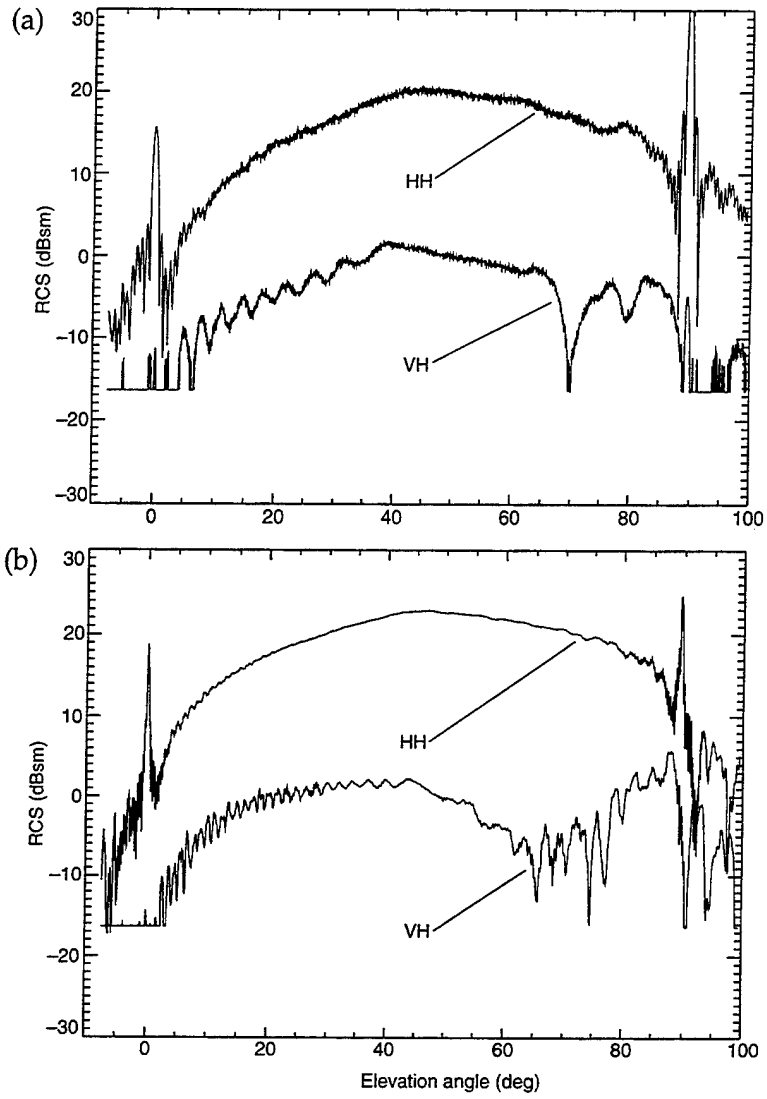

Figure 9. Measured bru03 RCS versus elevation angle at (a) 35 GHz and (b) 93 GHz.

If the PSMs for these reflectors were purely diagonal, the VV and HH amplitudes were the same, and the signals returned to the xpol-receive channels were due just to the finite orthogonal component admixture in the radars' transmissions, the shape of the RCS versus angle for xpol would be the same as that for copol. The lower cutoff and oscillatory nature of the top hat, 93-GHz xpol data in figure 6(b) and the lower cutoff of the bru02 xpol data of figure 11(a) make it difficult to compare their shape with that of the copol data in those figures. However, the shapes of the xpol data for bru01a in figure 7, for bru01 in figure 8(a), for bru03 in figures 9(a) and (b), and for bru02 in figure 10(a), for θ_{el} between about 20 and 45 degrees, do largely resemble those of the corresponding copol data. The shapes of the bru03 xpol data above 45 degrees, the top hat xpol data at 35 GHz, and the bru01 xpol data at 93 GHz are not understood.

Figures 12 and 13 show the RCS versus θ_{az} data at θ_{el} = 45 degrees for bru01 and bru02, respectively, the latter having been measured only at

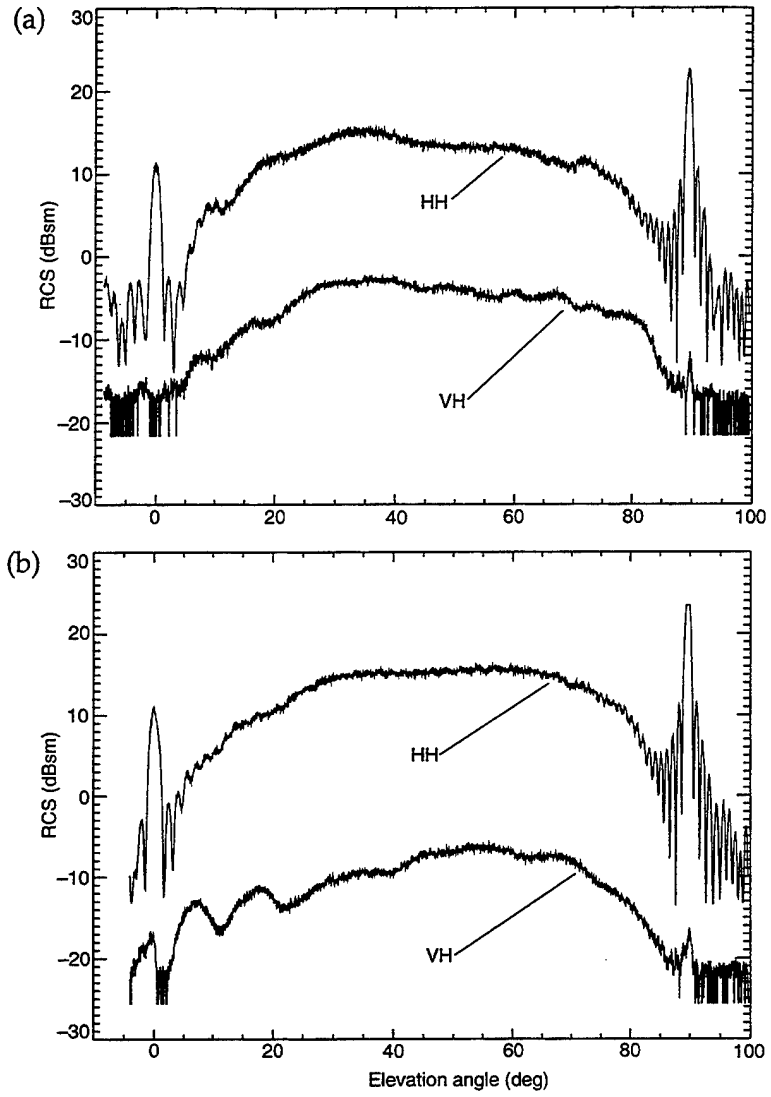

Figure 10. Bru02 RCS versus elevation at 35 GHz measured on different occasions.

93 GHz. The 93-GHz measurements for both Bruderhedrals exhibit a central portion oscillating about a "dc" value, and sidelobes whose peak values drop off rapidly as θ_{az} gets farther away from 0 degrees. The 10-dB (relative to the dc value) widths of these central portions are 3.4 degrees for bru01 and 9.2 degrees for bru02. These are similar to the values of $\alpha = 4$ degrees and 11 degrees, given for bru01 and bru02, respectively, in table 1. An RCS versus θ_{az} pattern similar in shape to the approximately "flat-topped" one of the central lobe of the bru01 patterns at 93 GHz has also been observed by Bruder [5], although his data do not exhibit a sidelobe pattern.

The data of figures 12 and 13 show that in using these reflectors for calibration, the orientation in the azimuthal plane is even more critical than that cited above for the elevation plane. Thus, in order not to incur a calibration uncertainty of more than 1 dB, the deviation in θ_{az} from 0 degrees for bru01 at either 35 or 93 GHz and for bru02 at 93 GHz may not be more than 0.5 degrees.

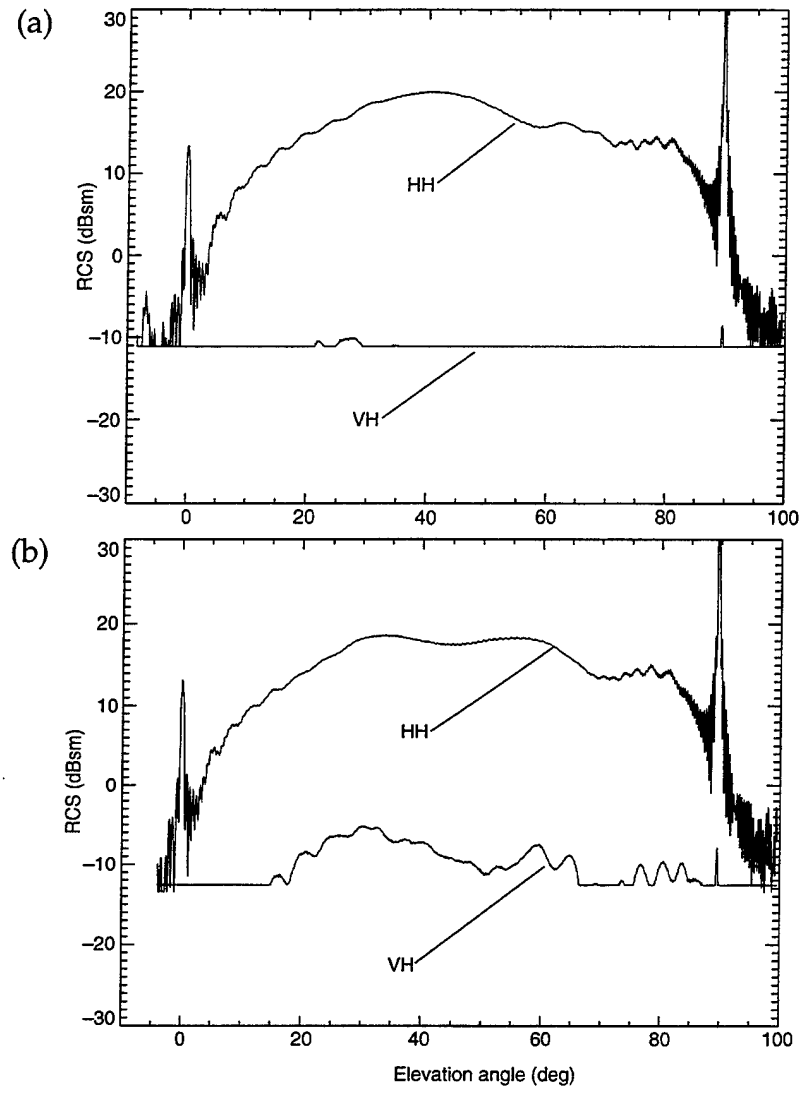

Figure 11. Bru02 RCS versus elevation at 93 GHz measured on different occasions.

The cylinder segments of these Bruderhedrals deviate from flatness only by an amount of the order of one wavelength or less at both 35 and 93 GHz. Therefore, based upon what is known about the RCS versus θ_{az} of plane dihedrals [5], one might expect there to be some similarities between the shapes of Bruderhedral RCS versus θ_{az} patterns and that of the RCS versus angle of incidence near normal incidence of a flat plate having dimensions similar to those of the Bruderhedrals. The physical optics treatment of the flat plate RCS has been well documented [5]. Figure 14, which shows plots of this RCS for a 6- × 6-in square plate at 35 and 93 GHz, bears out our expectations. The detailed shapes of the central and sidelobe structures in figures 12 and 13 might be explained by convolutions in angle space of the flat plate patterns in figure 14, with appropriate optical-like patterns for "apertures" corresponding to 4.3 degrees and 11.4 degrees for bru01 and bru02, respectively.

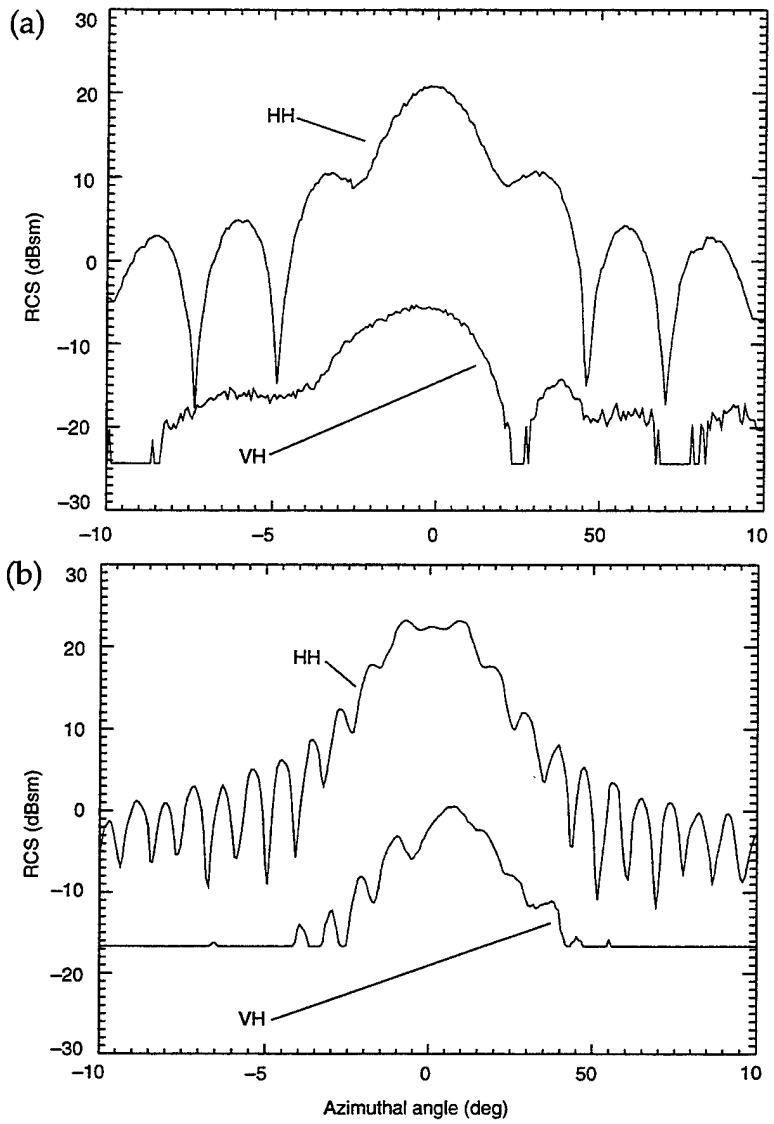

Figure 12. Measured bru01 RCS versus azimuthal angle at (a) 35 GHz and (b) 93 GHz.

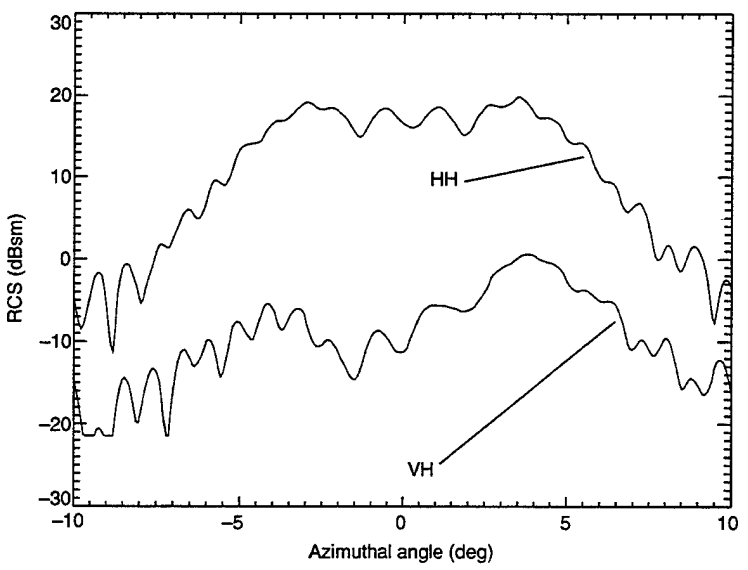

Figure 13. Measured bru02 RCS versus azimuthal angle at 93 GHz.

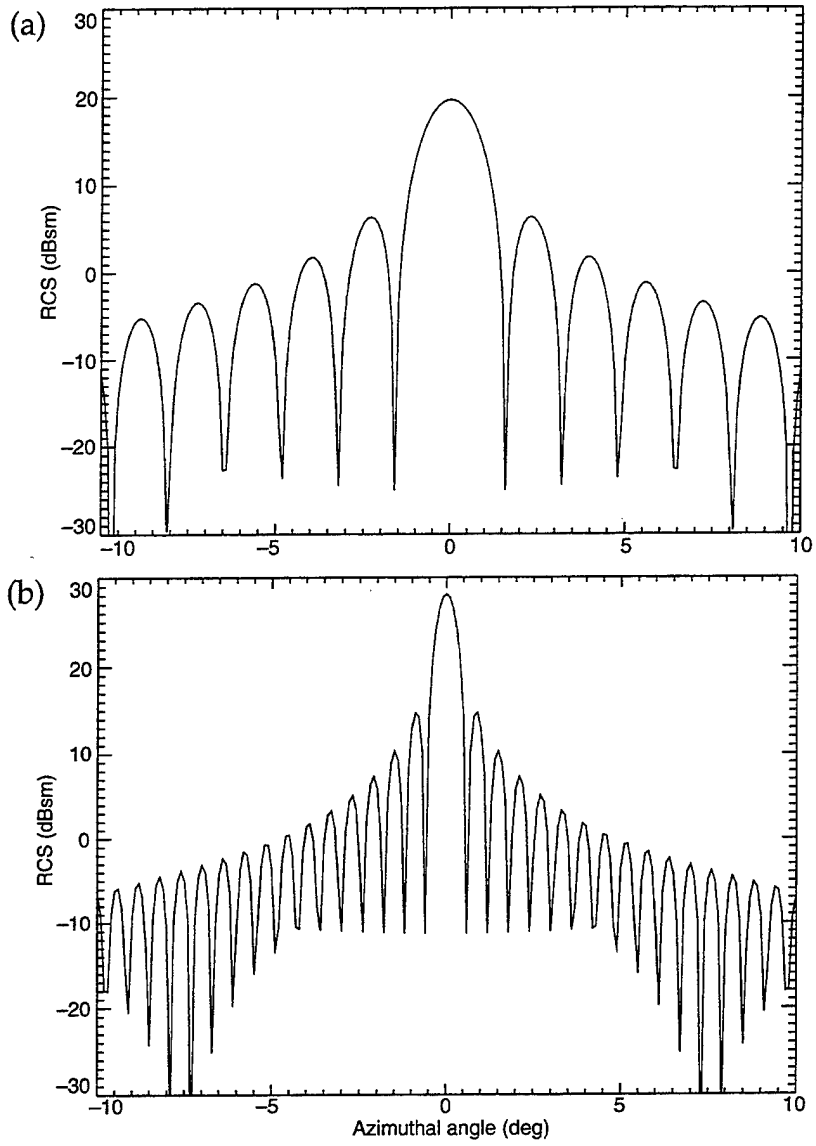

Figure 14. Calculated RCS versus angle of RLOS to normal for 6- × 6-in. square plate at (a) 35 GHz and (b) 93 GHz.

5. Comparisons of Measured Data With Predictions

5.1 RCS versus Elevation Angle

Figures 15 through 18 compare the measured HH RCS versus θ_{el} over the range of 10 to 80 degrees with the predictions of the theories and codes described in section 2. These comparisons are not made for the bru02 data, however, because of the inconsistent results obtained for these measurements noted in section 4.

We obtained xpatch results shown in figures 15 through 18 using xpatch2. These simulations included the effects of ray divergence and edge diffraction. As described in section 2, RCS simulations were also made with xpatch1. These included the effect of ray divergence, but were carried out both with and without the inclusion of edge diffraction. The overall agreement of the xpatch1 simulation results with the measured results was about the same as that of the xpatch2 results.

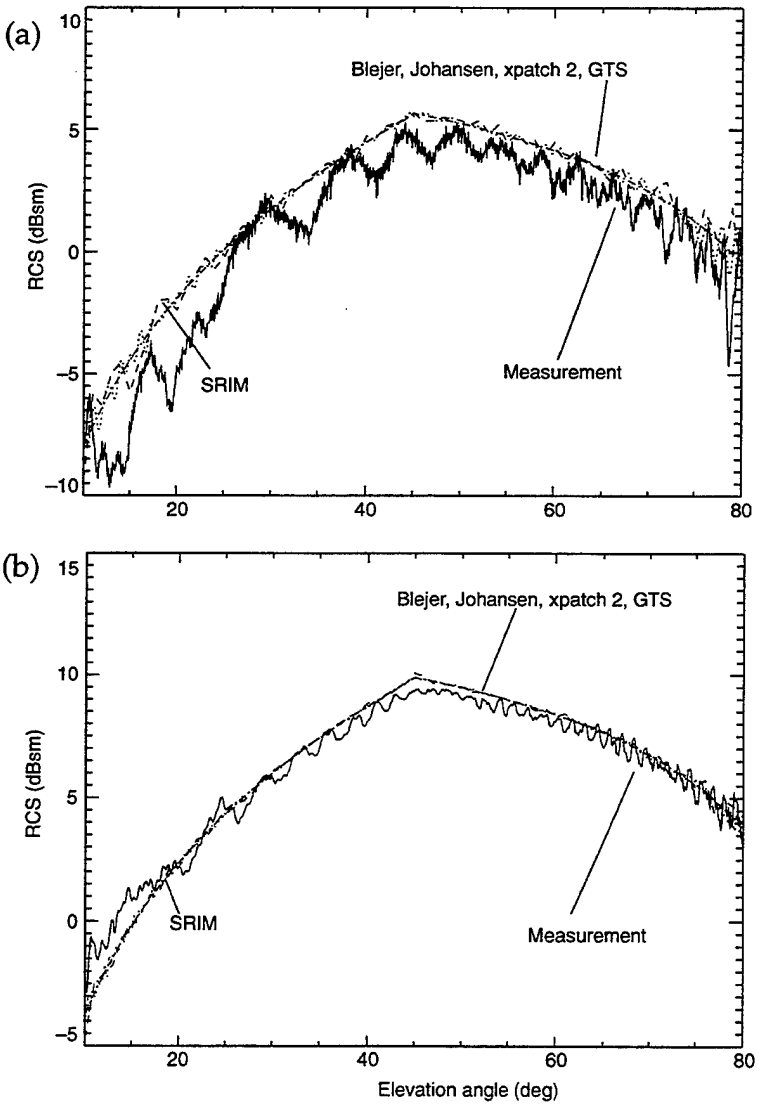

Figure 15. Measurements and predictions of top hat RCS versus elevation angle at (a) 35 GHz and (b) 93 GHz.

Figure 16. Measurements and predictions of bru01a, HH RCS versus elevation angle at 93 GHz.

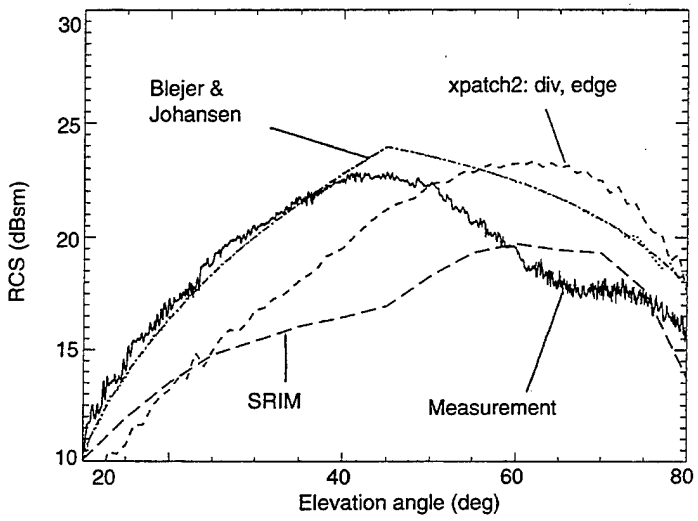

Figure 17. Measurements and predictions of bru01, HH RCS versus elevation angle at (a) 35 GHz and (b) 93 GHz.

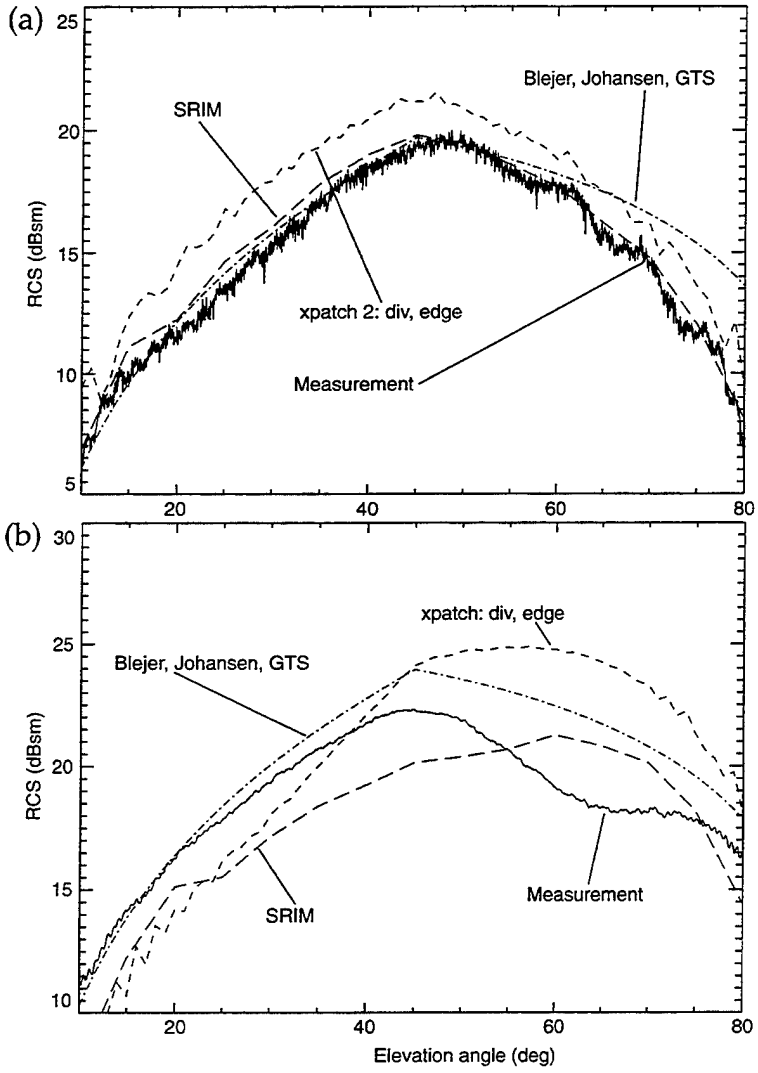

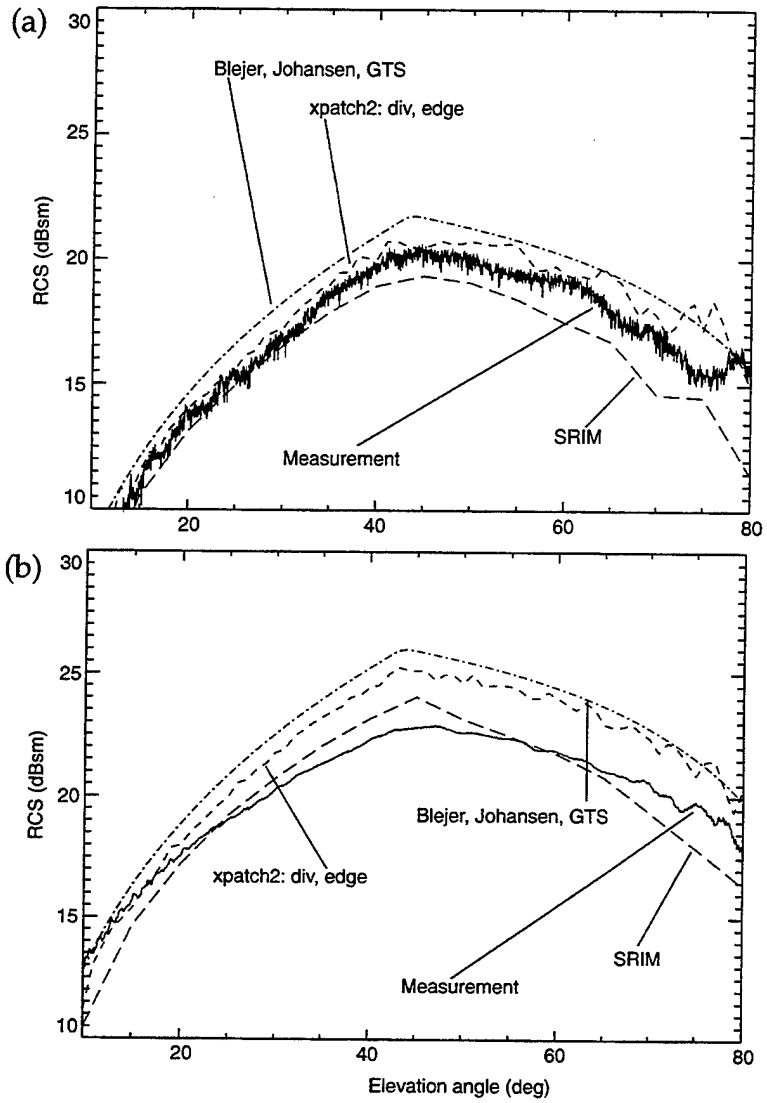

Figure 18. Measurements and predictions of bru03, HH RCS versus elevation angle at (a) 35 GHz and (b) 93 GHz.

Referring to table 1 (see p 9), it is seen that the dimensions of the top hat are sufficiently larger than λ at both 35 GHz and 93 GHz for the last three matrix elements to be neglected on the right-hand side of equation (7) for Blejer's theory. Therefore, neither the Blejer theory results in figure 15(a) nor those in figure 15(b) display any sizable oscillations. The same is true for the xpatch and GTS results. However, the figures show that, unlike these theoretical predictions, the RCS measurements on the top hat display rather large oscillations, with amplitudes on the order of 3 dB at 35 GHz (fig. 15(a)) and 1 dB at 93 GHz (fig. 15(b)). Furthermore, the agreement of the measured RCS with that predicted by the Blejer theory for the OSU top hat, shown in figure 2(b), is seen to be much better than that for the top hat measured in this work, shown in figure 15. In view of the discussion of the Blejer theory in section 2, this latter result is surprising, since the dimensions of the former top hat compared to λ ($a/\lambda = 3$, $b/\lambda = 7$, $L/\lambda = 3$) are smaller than those of the latter top hat at either 35 GHz or 93 GHz (table 1).

The results of the GTS code are practically identical to those of the Johansen and Blejer theories for all the reflectors. This is perhaps not surprising, since, like those theories, GTS uses both geometric optics and physical optics to calculate the lowest-order scattered fields from the primitives making up the target [18]. Figure 17(b) shows that none of the theories or simulations predicts the broad dip in the bru01 RCS measured between θ_{el} values of 55 and 75 degrees.

Tables 2 and 3 summarize the extent of agreement between the measured and computed HH RCS discussed above. Table 2 gives the difference, expressed in dB, between the maximum RCS measured in the θ_{el} range of 10 to 80 degrees and the maximum RCS predicted in that range. Table 3 gives the root-mean-squared (rms) difference between the measured RCS and predicted RCS over that same range in θ_{el}, obtained by comparing each measured data point in that range with the corresponding predicted value. Since the estimated standard deviation of the measured RCS is about 1 dB, an entry in these tables of that amount can be taken to signify complete agreement.

The results of table 2 have direct practical significance, since, in using these reflectors for calibration purposes, it is convenient to orient them for maximum return. Because of the oscillatory nature of the top hat measured data, especially at 35 GHz, its results were based on estimates of the "dc" value of the measured data in figure 15. The result of these estimates is that all the predictions of the maximum top hat RCS, except those of SRIM, agree with the measured values within 1 dB. For the Bruderhedrals, all the predicted maximum RCS values are within 2 dB of the measured ones, except for predictions of the theories and GTS for bru03 at 93 GHz, which deviate from the measured values by 3 dB.

Table 2. Comparison of measured maximum RCS to calculated maximum RCS.

RCS difference (dB) between measured maximum RCS and predicted maximum RCS in the elevation angle range of 10 to 80 degrees.

	Top hat		bru01		bru03	
Model	35 GHz	93 GHz	35 GHz	93 GHz	35 GHz	93 GHz
Blejer/Johansen	1	1	0	1	1	3
Johansen						
GTS	1	1	0	1	2	3
xpatch2	1	1	2	2	0	2
SRIM	–3	–3	0	–2	–1	1

Table 3. Overall comparisons of measured RCS to calculated RCS.

RMS difference (dB) between measured RCS and predicted RCS over elevation angle range of 10 to 80 degrees.

	Top hat		bru01		bru03	
Model	35 GHz	93 GHz	35 GHz	93 GHz	35 GHz	93 GHz
Johansen	2	1	2	2	2	2
Blejer	2	1	2	1	1	2
GTS	2	1	2	2	1	2
xpatch2	2	1	2	3	1	2
SRIM	2	2	1	2	1	1

Since table 3 gives rms values, its top hat data are probably numerically correct, even though the measured top hat data are oscillatory, since many oscillations occur throughout the 10- to 80-degree range in θ_{el}. The predictions for all the reflectors agree overall with the corresponding measured data to within 2 dB, except for the 93-GHz prediction of SRIM for the top hat and the 93-GHz prediction of xpatch2 for bru01, which are within 3 dB.

The predicted differences between the maximum HH RCS and the maximum VV RCS were almost always within 1 dB, in agreement with the measured values at 93 GHz. Table 4 gives the measured maximum and predicted maximum VH RCS, respectively, for all the reflectors. As was to be expected, based on the general reciprocity theorem [19], HV RCS values measured at 93 GHz were nearly the same as VH values measured at 93 GHz. Based on a physical optics treatment at MMW frequencies of the plane dihedral [17], when that reflector is oriented parallel or perpendicular to the polarization vector and has dimensions that are large compared to λ, as was the case for the reflectors in this work, the xpol RCS for that reflector should be extremely small. The very small values in table 4 therefore imply that, polarimetrically, the top hat and Bruderhedral are very similar to the plane dihedral. For the top hat and bru01, the maximum measured VH RCS may be attributed to a finite orthogonal admixture in the radar's polarization; the existence of a possible significant xpol RCS; or, what is most likely, a slight misalignment, whose effects would be more pronounced in xpol channels than in copol channels. The finite simulated VH RCS may be attributed to computational artifacts, such as roundoff error.

5.2 RCS versus Azimuthal Angle

Figure 19 compares measurements of the HH RCS versus θ_{az} at θ_{el} = 45 degrees for bru01 at 35 and 93 GHz with xpatch and SRIM predictions, and figure 20 does the same at 93 GHz for bru02. In all cases, the central lobes predicted by the codes are wider than the measured ones, but similar to them in shape and amplitude.

The codes predict sidelobes for bru01 that are wider than the measured ones, and they predict practically no sidelobes at all for bru02.

Table 4. Maximum VH RCS.

Maximum RCS (dBsm).

Source of values	Top hat		bru01		bru02		bru03	
	35 GHz	93 GHz	35 GHz	93 GHz	35 GHz	93 GHz	35 GHz	95 GHz
Measured	–13	–20	0	–8	*	*	2	2
Blejer	*	*	*	*	*	*	*	*
GTS	*	*	*	*	*	*	*	*
xpatch2	–60	–70	–40	–40	–42	–80	–20	–35
SRIM	–95	–81	–104	–51	–100	–89	–34	–34

**No VH predicted or measured.*

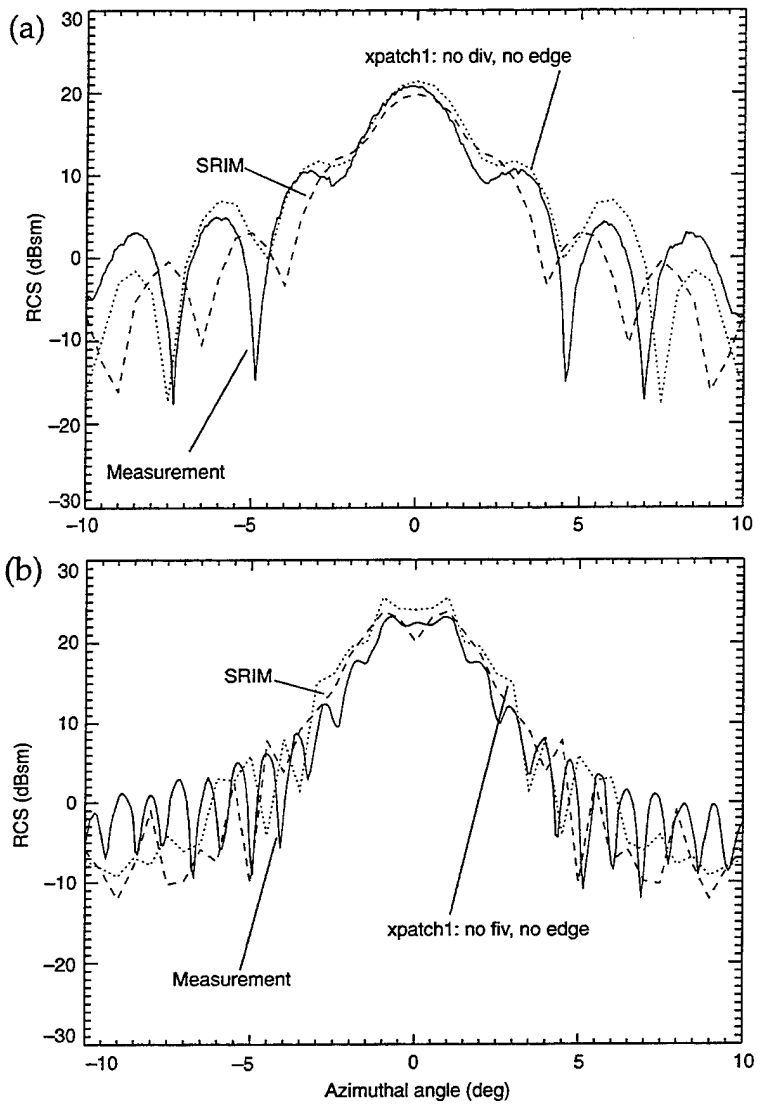

Figure 19. Measurements and predictions of bru01, HH RCS versus azimuthal angle at (a) 35 GHz and (b) 93 GHz.

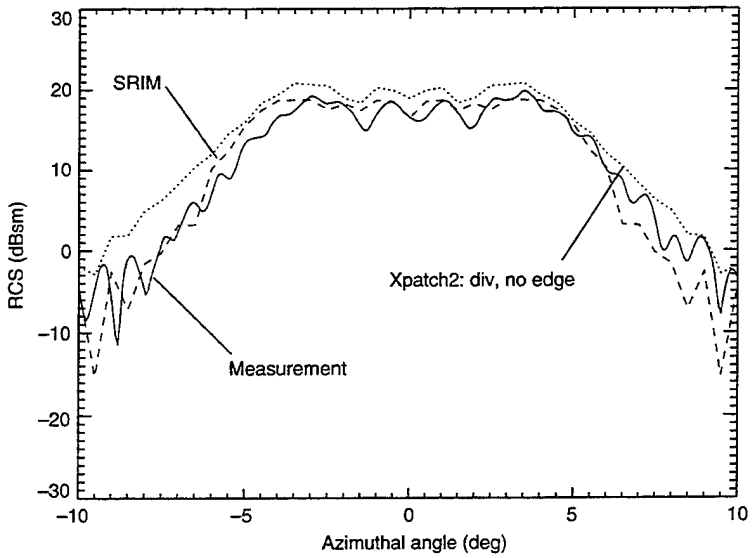

Figure 20. Measurements and predictions of bru02, HH RCS versus azimuthal angle at 93 GHz.

6. Conclusions

Our experiences in the course of measuring the RCS data described herein, and the extent of agreement between the results of those measurements and theoretical predictions, lead to the following conclusions:

1. A prediction of the maximum copol RCS of a given top hat or Bruderhedral at millimeter wavelengths based solely on the Johansen or Blejer theories, or the GTS, xpatch, or SRIM codes is not, in general, reliable to better than 3 dB.

2. One may determine the RCS of those reflectors with a reliability closer to 1 dB by making direct measurements. However, the following special provisions for care in making those measurements must be taken in addition to "standard" ones.

   a. Take special care in aligning the reflector with the RLOS every time the reflector is remounted. A three-axis mount would be very desirable.

   b. Make repeated absolute calibration measurements on a "well-understood" reflector, such as a sphere, cylinder, or trihedral for copol and a dihedral for xpol.

   c. Perform the calibrations in 2(b) before and after each set of measurements of the relative return signal from the reflector versus elevation angle.

3. To achieve calibrations of a radar reliable to nearly 1 dB using these reflectors, one must be able to control the orientations of the reflectors relative to the RLOS to about 5 degrees in the θ_{el} plane, and to as little as 0.5 degrees in the θ_{az} plane.

4. All the above theories and codes predict a shape of the reflector copol RCS at millimeter wavelengths for $10° < \theta_{el} < 80°$ that is almost identical to the measured one for a top hat, but not for a Bruderhedral. The shapes predicted by SRIM for any of those reflectors may or may not be reliable.

5. The measured xpol RCS is very small relative to the measured copol RCS, consistent with predictions of the theories and codes.

References

1. E. Johansen, *Top-Hat Reflectors Cap Radar Calibration*, Microwaves, pp 65-66 (December 1981).

2. R. M. Barnes, *Polarimetric Calibration Using In-Scene Reflectors*, Project Report TT-65, Massachusetts Institute of Technology, Lincoln Laboratory, Lexington, MA (10 September 1986).

3. D. J. Blejer, *Physical Optics Polarization for a Top Hat Reflector*, IEEE Trans. on Ant. and Prop., **39**, No. 6, pp 857-859 (June 1991).

4. N. Akhter and R. J. Marhefka, *Far Zone Electromagnetic Scattering From Complex Shapes Using Geometrical Theory of Diffraction*, Report WL-93-1030, U.S. Air Force Wright Laboratory, Wright Air Force Base, OH (December 1992).

5. R. N. Trebits, "Radar Cross Section," in *Radar Reflectivity Measurement: Techniques & Applications*, Chap. 2, edited by N. C. Currie, Artech House, Norwood, MA (1989).

6. J. A. Bruder, T. L. Lane, M. M. Horst, B. E. Huitt, S. W. Parker, and J. A. Scheer, *Tower Measurements of U.S. Vehicles TABILS Users Manual*, U.S. Army MICOM Technical Report CR-RD-AS-87, Redstone Arsenal, AL (July 1987).

7. R. J. Wellman, D. R. Hutchins, J. L. Silvious, H. Dropkin, G. Goldman, J. Nemarich, D. A. Wikner, and R. K. Dahlstrom, *Radar Cross Sections of Ground Clutter at 95 GHz for Summer and Fall Conditions*, NATO AGARD Conference Proceedings, Palma de Mallorca, Spain (May 1993).

8. N. C. Currie and G. W. Ewell, "Radar Cross Section Measurement Concepts," in *Radar Reflectivity Measurement: Techniques & Applications*, Chap. 3, edited by N. C. Currie, Artech House, Norwood, MA (1989).

9. J. Bruder, Georgia Tech Research Institute/SEAL, Smyrna, GA, private communication.

10. M. Walsh and C. L. Arnold, Jr., *SRIM User Reference Manual, Release 4.0*, Environmental Research Institute of Michigan Technical Report 212100-17-T, Ann Arbor, MI (January 1991).

11. D. J. Andersh, M. Hazlett, S. W. Lee, D. D. Reeves, D. P. Sullivan, and Y. Chu, *XPATCH, A High-Frequency Electromagnetic-Scattering Prediction Code and Environment for Complex Three-Dimensional Objects*, IEEE Antennas and Propagation Magazine **36**, pp 65-69 (February 1994).

12. TRACK/GTS, developed by Georgia Tech Research Institute, distributed by U.S. Navy, Naval Sea Systems Command, Washington, DC.

13. C. L. Arnold, Jr., ERIM, Ann Arbor, MI, private communication.

14. The Ballistic Research Laboratory CAD Package Release 4.0, U.S. Army Research Laboratory, Advanced Computational & Information Sciences Directorate, Aberdeen Proving Ground, MD (December 1991).

15. P. Cremona-Simmons, *An Analytical Characterization of a Known Calibration Target*, Army Research Laboratory, ARL-MR-241 (September 1995).

16. Spectrum Technologies International, Inc., Norcross, GA.

17. J. Verly, *Physical Optics Polarization Scattering Matrix For A Right-Angle Dihedral*, Technical Report 1008, Massachusetts Institute of Technology, Lincoln Laboratory, Lexington, MA (7 February 1995).

18. S. Carter, National Ground Intelligence Center, Charlottesville, VA; private communication.

19. J. L. Eaves and E. K. Reedy, editors, *Principles of Modern Radar*, Van Nostrand Reinhold, New York, p 628 (1987).

Acknowledgments

The authors acknowledge the support in this work they received from Peter Cremona-Simmons of the Army Research Laboratory (ARL), who constructed the faceted models; from Steve L. Carter of the National Ground Intelligence Center, who ran the GTS simulations; and from J. Nemarich, H. B. Wallace, and H. Dropkin, also of ARL, who made many suggestions in the course of stimulating discussions.

Appendix A.— Extension of Johansen's Theory

Figure A-1(a) depicts the bistatic scattering at wavelength, l, from a right circular cylinder of radius, a, and length, b. Based on equation (1) and a known relationship between monostatic and bistatic scattering,[1] the bistatic RCS, σ_{bi}, is

$$\sigma_{bi} = 2\pi a b^2 \cos(\theta_{el})/\lambda \ . \qquad \text{(A-1)}$$

When $\theta_{el} = 0$ degrees, equation (A-1) reduces to equation (1) in the main body of the report, as, of course, it must.

Figures A-1(b) and A-1(c) depict the scattering from a top hat based on the above right circular cylinder. These figures show that the effective cylinder height, b_{eff}, is

$$b_{eff} = 2\,L\,\tan(\theta_{el}), \text{ for } \tan(\theta_{el}) \le b/L \ , \qquad \text{(A-2)}$$

and

$$b_{eff} = 2b, \text{ for } \tan(\theta_{el}) \ge b/L \ . \qquad \text{(A-3)}$$

The factor 2 in equations (A-2) and (A-3) comes about because the top hat specular scattering field consists of two components of equal magnitude and phase: one due to scattering from the cylinder toward the base, and the other due to scattering from the mirror image of the cylinder in the base toward the cylinder.

We postulate that, based on equation (A-1), the top hat RCS is

$$\sigma = 2\pi a\,(b_{eff})^2 \cos(\theta_{el})/\lambda \ . \qquad \text{(A-4)}$$

Substituting equations (A-2) and (A-3) into equation (A-4), we obtain the top hat RCS given in equations (5) and (2) of section 2 in the main body of the report, respectively.

[1] G. W. Ewell, "Bistatic Radar Cross Section Measurements," in *Radar Reflectivity Measurements: Techniques & Applications*, Chap. 5, edited by N. C. Currie, Artech House, Norwood, MA (1989).

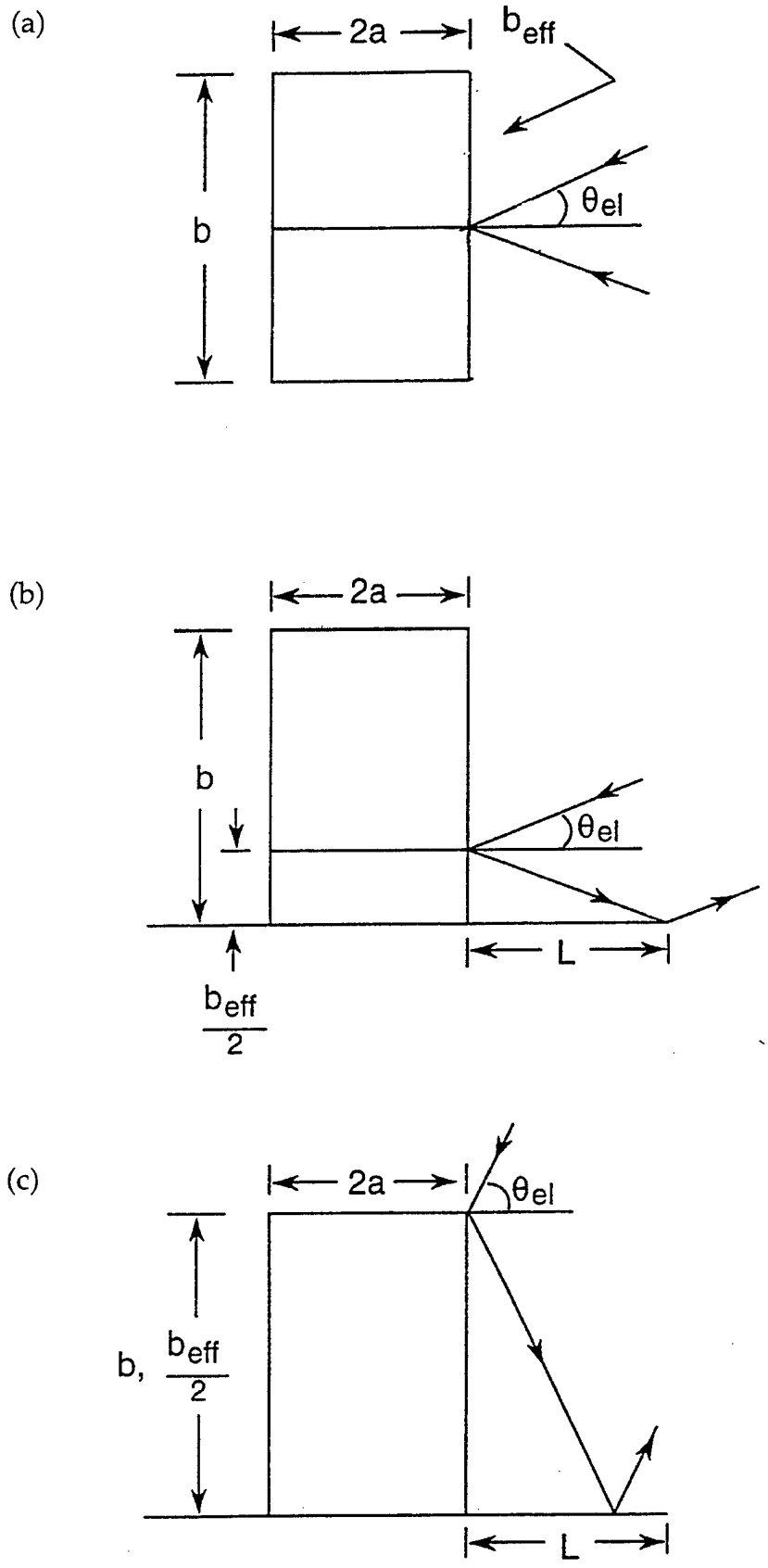

Figure A-1. Depictions of scattering from reflectors based on finite right circular cylinder. Figure shows (a) bistatic scattering from right circular cylinder, (b) backscattering from top hat with tan $(\theta_{el}) \leq b/L$, and (c) backscattering from top hat with tan $(\theta_{el}) \geq b/L$.

Distribution

Admnstr
Defns Techl Info Ctr
Attn DTIC-OCP 1
8725 John J Kingman Rd Ste 0944
FT Belvoir VA 22060-6218

Minister of Defense
Attn A Priou
Paris France

Under Secy of Defns for Rsrch & Engrg
Attn Rsrch & Advncd Techlgy
Depart of Defns
Washington DC 20310

CECOM
Attn PM GPS COL S Young
FT Monmouth NJ 07703

CECOM NVESD
Attn AMSEL-RD-NV-ASD M Kelley
Attn AMSEL-RD-NV-TISD F Petito
Attn Techl Lib
FT Belvoir VA 22060

CECOM
Sp & Terrestrial Commctn Div
Attn AMSEL-RD-ST-MC-M H Soicher
FT Monmouth NJ 07703-5203

DARPA
Attn B Kaspar
Attn J Pennella
Attn L Stotts
3701 N Fairfax Dr
Arlington VA 22203-1714

Dpty Assist Scy for Rsrch & Techl
Attn SARD-TT D Chait
Attn SARD-TT F Milton Rm 3E479

Dpty Assist Scy for Rsrch & Techl (cont'd)
Attn SARD-TT K Kominos
Attn SARD-TT R Reisman
Attn SARD-TT T Killion
The Pentagon
Washington DC 20310-0103

US Army Matl Cmnd
Dpty CG for RDE Hdqtrs
Attn AMCRD BG Beauchamp
5001 Eisenhower Ave
Alexandria VA 22333-0001

DUSD Space
Attn 1E765 J G McNeff
3900 Defense Pentagon
Washington DC 20301-3900

Hdqtrs Dept of the Army
Attn DAMO-FDQ D Schmidt
400 Army Pentagon
Washington DC 20310-0460

NGIC
Attn Iang RSC S Carter
Charlottesville VA 22902-5396

OSD
Attn OUSD(A&T)/ODDDR&E(R) J Lupo
The Pentagon
Washington DC 20301-7100

US Army Matl Cmnd
Prin Dpty for Acquisition Hdqrts
Attn AMCDCG-A D Adams
Attn AMCDCG-T M Fisette
5001 Eisenhower Ave
Alexandria VA 22333-0001

US Army Armament RDE Ctr
Attn SMCAR-FSP-A1 M Rosenbluth
Attn SMCAR-FSP-A1 R Collett
Picatinny Arsenal NJ 07806-5000

US Army CECOM NVESD
Attn AMSEL-RD-NV-RSPO A Tarbell
Attn AMSEL-RD-SR-R J Borowick
Mailstop 1112
FT Monmouth NJ 07703-5000

US Army Materiel Command
Attn AMCDM Dir for Plans & Analysis
5002 Eisenhower Ave
Alexandria VA 22333-0001

Distribution

US Army Missile Lab
Attn AMSMI-RD Advanced Sensors Dir
Attn AMSMI-RD Sys Simulation & Dev Dir
Attn AMSMI-RD-AS-MM G Emmons
Attn AMSMI-RD-AS-MM H Green
Attn AMSMI-RD-AS-MM M Christian
Attn AMSMI-RD-AS-MM M Mullins
Attn AMSMI-RD-AS-MM S Mobley
Attn AMSMI-RD-AS-MM W Garner
Attn AMSMI-RD-AS-RPR Redstone Sci Info Ctr
Attn AMSMI-RD-AS-RPT Techl Info Div
Redstone Arsenal AL 35809

US Army Rsrch Ofc
Attn B D Guenther
Attn C Church
PO Box 12211
Research Triangle Park NC 27709-2211

US Army Test & Evaluation Cmnd
Attn STEWS-TE-AF F Moreno
Attn STEWS-TE-LG S Dickerson
White Sands Missile Range NM 88002

US Military Academy
Dept of Mathematical Sci
Attn MAJ D Engen
West Point NY 10996

USA CRREL
Attn G D Ashton
Attn SWOE G Koenig

USA CRREL (cont'd)
Attn SWOE P Welsh
72 Lyme Rd
Hanover NH 03755

USAASA
Attn MOAS-AI W Parron
9325 Gunston Rd Ste N319
FT Belvoir VA 22060-5582

USAE Waterways Exprmnt Sta
Attn CEWES-EE-S J Curtis
Attn CEWES-EN-C W West
3909 Halls Ferry Rd
Vicksburg MS 39180-6199

USATEC
Attn J N Rinker
Attn P Johnson
7701 Telegraph Rd
Alexandria VA 22315-3864

Nav Rsrch Lab
Attn 2600 Techl Info Div
4555 Overlook Ave SW
Washington DC 20375

Nav Surface Weapons Ctr
Attn DX-21 Library Div
Dahlgren VA 22448

Nav Weapons Ctr
Attn 38 Rsrch Dept
Attn 381 Physics Div
China Lake CA 93555

AFMC Rome LAB/OC 1
Attn J Bruder
Griffiss AFB NY 13441-4314

Eglin Air Force Base
Attn 46 TW/TSWM B Parnell
211 W Eglin Blvd Ste 128
Eglin AFB FL 32542-5000

GPS Joint Prog Ofc Dir
Attn COL J Clay
2435 Vela Way Ste 1613
Los Angeles AFB CA 90245-5500

Special Assist to the Wing Cmndr
Attn 50SW/CCX CAPT P H Bernstein
300 O'Malley Ave Ste 20
Falcon AFB CO 80912-3020

Distribution

USAF SMC/CED
Attn DMA/JPO M Ison
2435 Vela Way Ste 1613
Los Angeles AFB CA 90245-5500

USAFWright Lab
Attn WL/MMGS B Sundstrum
Attn WL/MMGS R Smith
101 W. Eglin Blvd Ste 287A
Eglin AFB FL 32542-6810

Sandia Natl Lab
PO Box 5800
Albuquerque NM 87185

University of TX
ARL Electromag Group
Attn Campus Mail Code F0250 A Tucker
Austin TX 78712

Eviron Rsrch Inst of MI
Attn C L Arnold
PO Box 134001
Ann Arbor MI 48113-4001

Georgia Institite of Technology
Georgia Tech Rsrch Inst
Attn Radar & Instrmntn Lab R McMillan
Attn Radar & Instrmntn Lab T L Lane
Attn Radar & Inrmntn Lab N C Currie
Atlanta GA 30332

Ohio State Univ Elect Sci Lab
Attn R J Marhefka
Columbus OH 43212

Univ of Michigan Radiation Lab
Attn F Ulaby
Attn K Sarabandi
3228 EECS Bldg 1301 Beal Ave
Ann Arbor MI 48109-2122

VA Polytechnic Inst & State Univ
Elect Interaction Lab
Attn G S Brown
Bradley Dept of Elect Engrg
Blacksburg VA 24061-0111

CECOM RDEC
Electronic Systems Div Dir
Attn J Niemela
FT Monmouth NJ 07703

Lockheed Martin Corp
Elect & Missile Div
Attn E Weatherwax
5600 Sand Lake Rd Mail Stop 450
Orlando FL 32819

MIT Lincoln Lab
Attn E Austin
Attn W Keicher
PO Box 73
Lexington MA 02173-9108

Simulation Technl
Attn A V Saylor
Attn D P Barr
PO Box 7009
Huntsville AL 35807

US Army Rsrch Lab
Attn AMSRL-P-S-E B Perlman
FT Monmouth NJ 07703-5601

US Army Rsrch Lab
Attn AMSRL-WT-WB R A McGee
Aberdeen Proving Ground MD 21005

US Army Rsrch Lab
Attn AMSRL-CI-LL Tech Lib (3 copies)
Attn AMSRL-CS-AL-TA Mail & Records Mgmt
Attn AMSRL-CS-AL-TP Techl Pub
Attn AMSRL-SE J M Miller
Attn AMSRL-SE-D E Scannell
Attn AMSRL-SE-E D Wilmot
Attn AMSRL-SE-E J Pellegrino
Attn AMSRL-SE-EE Z G Sztankay
Attn AMSRL-SE-RM B Bender
Attn AMSRL-SE-RM B Wallace
Attn AMSRL-SE-RM C Ly
Attn AMSRL-SE-RM D Hutchins
Attn AMSRL-SE-RM D Wikner

Distribution

US Army Rsrch Lab (cont'd)
Attn AMSRL-SE-RM E Burke
Attn AMSRL-SE-RM G Goldman
Attn AMSRL-SE-RM H Dropkin
Attn AMSRL-SE-RM J Nemarich
Attn AMSRL-SE-RM J Silverstein
(20 copies)
Attn AMSRL-SE-RM J Silvious
Attn AMSRL-SE-RM
P Cremona-Simmons

US Army Rsrch Lab (cont'd)
Attn AMSRL-SE-RM R Dahlstrom
Attn AMSRL-SE-RM S Stratton
Attn AMSRL-SE-RU B Scheiner
Attn AMSRL-SE-RU J Sichina
Attn AMSRL-SE-SA R Wellman
Adelphi MD 20783-1197

REPORT DOCUMENTATION PAGE

Form Approved
OMB No. 0704-0188

1. AGENCY USE ONLY *(Leave blank)*	2. REPORT DATE	3. REPORT TYPE AND DATES COVERED
	March 1997	Final, from 1995 to 1996

4. TITLE AND SUBTITLE
Measurements and Calculations of the Millimeter Wavelength RCS of a Top Hat and Bruderhedrals

5. FUNDING NUMBERS
PE: 61102A

6. AUTHOR(S)
Joseph D. Silverstein and Robert Bender

7. PERFORMING ORGANIZATION NAME(S) AND ADDRESS(ES)
U.S. Army Research Laboratory
Attn: AMSRL-SE-RM
2800 Powder Mill Road
Adelphi, MD 20783-1197

8. PERFORMING ORGANIZATION REPORT NUMBER
ARL-TR-1281

9. SPONSORING/MONITORING AGENCY NAME(S) AND ADDRESS(ES)
U.S. Army Research Laboratory
2800 Powder Mill Road
Adelphi, MD 20783-1197

10. SPONSORING/MONITORING AGENCY REPORT NUMBER

11. SUPPLEMENTARY NOTES
AMS code: 611102.H43
ARL PR: 7NE2HH

12a. DISTRIBUTION/AVAILABILITY STATEMENT
Approved for public release; distribution unlimited.

12b. DISTRIBUTION CODE

13. ABSTRACT *(Maximum 200 words)*

Polarimetric radar cross sections (RCSs) were measured for a large top hat and three large Bruderhedrals at 35 and 93 GHz. The overall spread in the measured RCSs was 2 dB. It was found that the absolute RCS, as well as the dependence of the RCS on elevation angle, could be significantly altered by a slight misalignment of the target reflector. The calculations of these RCSs by theories and RCS simulation codes based on geometric and physical optics generally agreed with the measurements to within 3 dB. Radar calibrations using these reflectors, which are based on the predictions, are not reliable, however, if accuracy better than 3 dB is required. The measured values of the cross-polarization RCS were very small compared to the copolarization ones, consistent with theoretical predictions.

14. SUBJECT TERMS
Calibration, millimeter waves, radar cross section, reflectors

15. NUMBER OF PAGES
43

16. PRICE CODE

17. SECURITY CLASSIFICATION OF REPORT	18. SECURITY CLASSIFICATION OF THIS PAGE	19. SECURITY CLASSIFICATION OF ABSTRACT	20. LIMITATION OF ABSTRACT
Unclassified	Unclassified	Unclassified	UL

NSN 7540-01-280-5500

Standard Form 298 (Rev. 2-89)
Prescribed by ANSI Std. Z39-18
298-102